ResearchGate

See discussions, stats, and author profiles for this publication at: https://www.researchgate.net/publication/231683199

Thermodynamic and dynamic behavior of semiflexible polymers in the isotropic phase

ARTICLE *in* MACROMOLECULES · NOVEMBER 1991

Impact Factor: 5.8 · DOI: 10.1021/ma00023a014

CITATIONS
43

READS
14

2 AUTHORS, INCLUDING:

Paul Russo
Georgia Institute of Technology
131 PUBLICATIONS **2,321** CITATIONS

SEE PROFILE

Available from: Paul Russo
Retrieved on: 30 January 2016

Thermodynamic and Dynamic Behavior of Semiflexible Polymers in the Isotropic Phase

L. Mark DeLong† and Paul S. Russo*

Department of Chemistry and Macromolecular Studies Group, Louisiana State University, Baton Rouge, Louisiana 70803-1804

Received January 25, 1991; Revised Manuscript Received July 3, 1991

ABSTRACT: Static and dynamic light scattering measurements have been made for concentrated isotropic solutions of the semiflexible polymer poly(γ-benzyl α,L-glutamate) (PBLG) dispersed in *N,N*-dimethylformamide (DMF). Characterization of the fractionated polymers shows them to be reasonably monodisperse and quite stiff. The osmotic modulus, $(\partial\pi/\partial c)_{T,p}$, increases with concentration at very nearly the rate predicted long ago by Onsager, but sharp decreases are observed as the nematic transition is approached. The static correlation length decreases with concentration in the fashion proposed by Shimada, Doi, and Okano (*J. Chem. Phys.* **1988**, *88*, 2815) at low to moderate concentrations. At larger concentrations, the apparent correlation length decreases less rapidly than predicted and then actually increases. A a result, the scaling relation first proposed by de Gennes, Pincus, Velasco, and Brochard (*J. Phys. (Paris)* **1976**, *37*, 1461) is not obeyed precisely. The depolarized light scattering intensity, although quite weak in dilute solutions, increases markedly with concentration. The apparent molecular optical anisotropy increases in a fashion that is at least qualitatively consistent with the theory first proposed by Benoit and Stockmayer (*J. Phys. Radium* **1956**, *17*, 21). The average decay rates of intensity–intensity autocorrelation functions display the unusual angular dependence predicted by the random phase theory of Doi, Shimada, and Okano (*J. Chem. Phys.* **1988**, *88*, 4070). But the increase in apparent mutual diffusion coefficient is only about $^1/_3$ of that expected if the translational self-diffusion parallel to the rod axis is constant. Mutual friction coefficients increase monotonically with concentration. The initial rate of increase is consistent with the theory of Peterson (*J. Chem. Phys.* **1964**, *40*, 2640). It was possible to scale the friction coefficients with concentration using no adjustable parameters. While single-exponential autocorrelation functions were observed at low angles and concentrations, the decay spectrum at high concentrations contains at least three decay modes. Two of these exhibit qualitatively the behavior predicted by Shimada, Doi, and Okano (*J. Chem. Phys.* **1988**, *88*, 7181), with some exceptions.

I. Introduction

For more than 50 years, it has been known that solutions of rodlike microparticles exhibit a liquid crystalline phase when sufficiently concentrated.[1-4] The excluded volume origins of liquid crystallinity were identified by Onsager,[5] using a cluster expansion method. The most notable alternative is the Flory lattice model.[6-8] Either theory predicts a nematic transition in the absence of any specific polymer–solvent interactions, though they differ on the required concentration. The Flory theory, which can handle arbitrary solvent–polymer interactions, predicts a critical interaction parameter, $\chi_{crit} \approx 0$. Comparing this to random coils ($\chi_{crit} \approx {}^1/_2$) shows that, in the absence of polymer configurational entropy, very slightly unfavorable solvent–polymer enthalpic interactions can lead to demixing. Thus, a true solution of a rodlike polymer at substantial concentration is probably in the good-solvent limit. This accounts for the striking similarities in phase behavior for solutions of rods of many different chemical types.[9,10] Although limited to athermal systems, the simpler Onsager theory arrives at a useful expression for the osmotic second virial coefficient; it also argues against the importance of higher virial terms.

Variations on these theories have appeared (for a start, consult refs 11 and 12), but none addresses the issues of solution structure or dynamics. Recently, Doi, Shimada, and Okano (DSO) developed a random phase theory of rodlike polymers in isotropic solution.[13-15] Like Onsager, they carefully considered excluded volume in the athermal limit. It therefore comes as no surprise that key features of the Onsager theory are retrieved. However, an explicit purpose of the DSO approach is the computation of structure factors—including dynamic structure factors. Thus, in addition to thermodynamic information of a long-range nature, such as osmotic pressure, the DSO model pertains to equilibrium and dynamic predictions on a microscopic scale.

This paper explores thermodynamic and dynamic behavior of still polymers in solution from an experimental perspective. No rodlike polymer has all the characteristics desired for such a study, but synthetic polypeptides in helicogenic solvents are often chosen as model systems. In particular, poly(γ-benzyl α,L-glutamate) (PBLG) has been widely used.[16-20] Its synthetic pathway results in moderately narrow size distributions,[21] and PBLG is soluble as an uncharged molecule, without aggregation, in a few polar solvents, including especially dry *N,N*-dimethylformamide (DMF). The *bending* stiffness of PBLG, as judged by the persistence length,[22] a, is not known exactly.[18,23-29] But the *lowest* value reported, about 70 nm,[18] exceeds that of any other synthetic organic polymer,[28,29] including those with fully conjugated linear backbones.[10,28-30] Bending vibrations of individual bonds,[31] taken over many repeat units, may render such "true rods"[32] somewhat less rigid than helical structures, although high rigidity without any secondary structure is indeed a very remarkable achievement. PBLG undoubtedly has a much lower *longitudinal* modulus than the backbone-conjugated, linear polymers, one of many reasons it would be a poor choice for production of high-modulus fibers or other materials. But PBLG solutions offer perhaps the clearest window for observation of the fundamental behavior of rodlike particles in solution.

* To whom correspondence should be addressed.

† Work performed in partial fulfillment of the requirements for the Ph.D. degree, 1990. Present address: Union Carbide Corp., South Charleston, WV 25303.

0024-9297/91/2224-6139$02.50/0 © 1991 American Chemical Society

All solutions in this study are in the isotropic phase, but nondilute solutions are the main order of business. For one of us, it is the second article on scattering from binary solutions of PBLG in DMF. To place the earlier work[19] in perspective, we summarize the many improvements in the present paper: narrower PBLG fractions spanning a wider molecular weight range; greater completeness in the depolarized measurements; variation of temperature; and, more sophisticated analysis of the nonexponential character of the data. Most importantly, a thorough investigation of the static light scattering (SLS) has been made. There is nothing in the old data set[19] that is inconsistent with the present; however, the more extensive experiments, together with new theoretical insights, enable a much better interpretation.

II. Theoretical Background

(a) Static Light Scattering (SLS) in Solution. Neglecting depolarization effects, which are weak in the experiments to be discussed, the light scattered by a solution containing polymers at concentration c (weight/volume) is described by[33-35]

$$RTKc/\mathcal{R} = (\partial\pi/\partial c)_{T,p}(1 + \xi^2q^2 + ...) \quad (1)$$

The parameters on the left are all measurable or known. R is the gas constant and T is the absolute temperature. K is an optical constant: $K = 4\pi^2n^2(dn/dc)^2\lambda_0^{-4}\mathcal{N}^{-1}$, where n is the refractive index, (dn/dc) is the specific refractive index increment, λ_0 is the wavelength in vacuo, and $\mathcal{N}$ is Avogadro's number. The Rayleigh factor, $\mathcal{R}$, is proportional to the measured intensity.

Arranged on the right-hand side are the parameters of interest. The fundamental scattering power of the solution is inversely related to its osmotic modulus measured at constant temperature and pressure, $(\partial\pi/\partial c)_{T,p}$. This is mediated by interference arising from the various scattering elements, which is a series function of the product of the correlation length, ξ, and the modulus of the scattering vector, $q = 4\pi n \sin(\theta/2)/\lambda_0$, where θ is the scattering angle.

The osmotic modulus represents the resistance of a solution to concentration fluctuations. In high-modulus[36] solutions, fluctuations of low amplitudes lead to weak scattering. Low-modulus solutions—for example, near a liquid–liquid phase transition—give rise to greater scattering. For ordinary random coil polymers in good solvents, $(\partial\pi/\partial c)_{T,p}$ increases with c, as fluctuations away from the equilibrium average always involve crowding that becomes increasingly serious with c. In such systems, a decreasing osmotic modulus usually indicates poor solvent conditions. The situation is more complex for rodlike polymers, where the free energy of interaction depends not only on concentration but also on orientation. A striking result of theory and experiment is the coexistence of two phases with very different orientations, but similar concentrations. Thus, the coupling between orientation and concentration order parameters is weak, but finite. Such coupling is not confined to equilibrium phase boundaries; dynamic fluctuations in a single phase should likewise be linked. As a result, concentration fluctuations become large near the nematic transition, even in a good solvent. Decreasing $(\partial\pi/\partial c)_{T,p}$, particularly in the vicinity of the nematic transition, does not necessarily indicate a poor solvent condition for rods.

In dilute solution, the classical treatment of Zimm[35] yields

$$Kc/\mathcal{R} = M_w^{-1}(1 + q^2(R_g^2)_z/3 + ...) + 2A_2c + ... \quad (2)$$

where R_g is the radius of gyration ($=3^{1/2}\xi$ in the limit $c \to 0$). For a thin, rigid, monodisperse α-helix, R_g is calculated by

$$R_{g,calc}^2 = L^2/12 \quad (3)$$

where

$$L = h_\alpha M/M_0 \quad (4)$$

In eq 4, M_0 is the monomer molar mass, 219 g/mol for PBLG, and h_α is the translation per monomer repeat unit along the α-helix, 0.15 nm.

Zimm, Schulz, and Onsager[5,37,38] independently deduced A_2 in the continuum limit—i.e., assuming that the solvent particles are much smaller than the diameter, d, of the rods. In the absence of attractive forces, A_2 of thin, rigid rods is independent of molecular weight:

$$A_2 = (\pi\mathcal{N}/4)dL^2/M^2 \quad (5)$$

The expression is exact in the limit of infinite axial ratio, $x = L/d = \infty$.

(b) Random Phase Theory and Relationships to Other Models. The static structure factor $g(q)$, proportional to the intensity scattered per unit concentration, has been calculated for random coil polymers in solution using the random phase approximation (RPA).[39-41] To apply this self-consistent, mean field perturbation theory to rods, a "nematic potential" must be added to the usual excluded volume potential to account for orientation. In the mean field approximation, DSO showed that a generalized version of the RPA is analytically exact for perfectly rigid rods. For semiflexible polymers such as PBLG, RPA may work better than it does for flexible coils, where it is less successful than scaling theories.[14,42,43] However, in contrast to random coil polymers in good solvents where the mean field approximation improves with concentration, the nematic transition guarantees that there will be limits to the success of a mean field treatment of rods. Despite this, we have found the random phase theory to be quite useful. As the terminology changes slightly during the progression of the original three-part series—to be referred to as DSO-I,[13] DSO-II,[14] and DSO-III[15]—we review the main points and adopt a consistent nomenclature. At the same time, relationships to other theories will be identified, as will features that are readily tested by experiment.

Much of the theory revolves around the line segment density at a given point r, denoted by $\mathbf{c}(r)$. This has units of length^{-2} and must not be confused with c, which is the concentration expressed as weight/volume. The number density of polymers, $\nu = \mathcal{N}c/M$, is very important, for many experimental observations can be scaled when the concentrations are so described, as will become evident. Interactions among segments are described by the potential, $v_0 = \pi d/2$, and by the nematic interaction potential, $v_1 = (15/16)v_0$. The number-density osmotic second virial coefficient, $A_{2,\nu} = M^2A_2/\mathcal{N}$, satisfies the osmotic pressure relationship, $\pi = \nu k_BT(1 + \nu A_{2,\nu} + ...)$, where k_B is Boltzmann's constant. The Onsager–Zimm–Schulz value of $A_{2,\nu}$ in the excluded volume limit is $\pi dL^2/4$—the volume swept out by rotating a rod end over end about its midpoint.

Spontaneous formation of a nematic phase occurs at a number density inversely proportional to $A_{2,\nu}$. There are

at least four logical choices to define the critical concentration.[44] We select the concentration at which the local minimum for the isotropic state disappears from a plot of free energy vs orientation. This is

$$\nu^* = 4/A_{2,\nu} = 16/\pi dL^2 \tag{6}$$

The condition $\nu \approx \nu^*$ does approximately coincide with the onset of dramatic changes for solutions of PBLG/DMF. But phase separation is not among them. Actual formation of a stable lyotropic phase occurs at larger concentrations.

In Flory's original lattice treatment,[6] the critical polymer volume fraction, or "A point", at which the nematic phase first appears is estimated[7,8] as $\phi_A = (8/x)(1 - 2/x) \approx 8/x$ for large x. It is easily seen that this corresponds to $2\nu^*$. Ronca and Flory[7] argued that this large discrepancy results from the fundamental inability of cluster expansion theories to account for finite solvent size. This would cause A_2 to be overestimated, as will be explained heuristically in section IVb. Thus, there is some interest in whether or not experimentally determined virial coefficients are reasonable based on the expected dimensions of the molecule or independent measurements thereof.

Two equivalent expressions have been given for the static structure factor, $g(q)$, of concentrated rodlike polymers—eq 5.8 of DSO-I[13] and eq 3.22 of DSO-II.[14] The latter is reproduced below:

$$L/g(q) = 1 + 8\nu/\nu^* + (qL)^2/36 + \frac{7 - 27(\nu/\nu^*)}{32400(1 - \nu/\nu^*)}(qL)^4 + \dots \tag{7}$$

A few relationships will simplify comparison of equations in this paper, where concentrations are often scaled to ν^*, to the original DSO expressions where other reference concentrations are sometimes used. For example, comparison of eq 7 to eq 5.8 of DSO-I[13] shows that $\mathbf{c}L\upsilon_0 = 8\nu/\nu^*$. The parameter $\mathbf{c}_{\mathrm{ref}\,1}$ in the DSO papers, defined as $(a\upsilon_0)^{-1}$, represents the segment density at which a length a occupies a volume $a^2\upsilon_0 = \pi a^2 d/2$ (imagine two segments of length a confined to a disk of radius a and thickness d). This reference concentration, at which interaction should be significant if L is comparable to a, decreases with the stiffness and width of the polymer. Any concentration exceeds it for perfectly rigid rods ($a = \infty$). The relationship to ν^* is $\mathbf{c}/\mathbf{c}_{\mathrm{ref}\,1} = \mathbf{c}a\upsilon_0 = (a/L)(8\nu/\nu^*)$, which shows that $\mathbf{c}/\mathbf{c}_{\mathrm{ref}\,1}$ increases with stiffness and concentration. The crowded state just imagined at $\mathbf{c}_{\mathrm{ref}\,1}$ occurs when $\nu/\nu^* = {}^1/_8$ if $L = a$.

To eliminate the explicit L dependence from eq 7, we form the ratio

$$g(0)/g(q) = 1 + \frac{(qL)^2/36}{1 + 8\nu/\nu^*} + \frac{7 - 27(\nu/\nu^*)}{32400(1 - \nu/\nu^*)(1 + 8\nu/\nu^*)}(qL)^4 \tag{8}$$

$$= 1 + q^2\xi^2 + \mathcal{D}q^4 + \dots \tag{9}$$

Equation 9 is eq 5.1 in DSO-I.[13] The term $\mathcal{D}$ describes the deviation from linearity, or the curvature in a standard plot of $g(0)/g(q)$ against q^2 to determine ξ^2. If terms to q^2 are considered, then comparison of eqs 8 and 9 gives

$$(L/6\xi)^2 = 1 + 8\nu/\nu^* \tag{10}$$

Although first derived via the random phase theory, this expression is a natural consequence of simple, classical ideas (see Appendix). In the limit $\nu/\nu^* \gg {}^1/_8$, eq 10 implies

$$\xi \approx \nu^{-1/2} \approx c^{-1/2} \tag{11}$$

This relationship was first derived by de Gennes et al.[45] The same scaling relationship has been obtained for the hydrodynamic screening length.[46,47] The reduction in ξ with concentration is entirely described by the excluded volume effect—i.e., the υ_0 segment interaction term. This can be seen from eq 10 and the discussion following eq 7. In contrast, the fact that $\mathcal{D}$ changes sign from positive to negative as concentration is raised past $\nu/\nu^* = {}^7/_{27} \approx 0.26$ can be attributed entirely to the nematic interaction term.[14] Thus, the nematic interaction term affects only the q^4 coefficient. Except at high qL, it will be difficult to detect.

Finally, as ν approaches ν^*, eq 8 diverges at finite q, and accurate scattering envelopes cannot be computed. This represents the instability of the single isotropic phase. The scattering envelopes should drop off very rapidly with q at this point, representing long-range concentration correlations associated with the imminent phase transition. The divergent behavior emphasizes that the DSO model is fundamentally a theory of the stable isotropic phase, even though an objective of DSO-III is to describe the nematic transition.

(c) Dynamic Light Scattering (DLS) in Dilute Solutions. In the long-wavelength limit, the decay of the electric field autocorrelation function $g^{(1)}(\tau)$[48] is dominated by translational diffusion:

$$g^{(1)}(\tau) = \exp(-D_{\mathrm{m}}q^2\tau) \tag{12}$$

The appearance of the mutual diffusion coefficient, D_{m}, stresses that DLS senses concentration fluctuations—albeit very small random ones driven only by thermal energy. D_{m} is fundamentally different from the self-diffusion coefficient, D_{s}. The mutual diffusion coefficient is described by[49-51]

$$D_{\mathrm{m}} \approx (M/\mathcal{N})(\partial\pi/\partial c)_{T,p}/f_{\mathrm{m}} \tag{13}$$

Equation 13 neglects a term of $1 - \phi$, where ϕ is the fraction of solution volume occupied by polymer, which in the present case leads to errors <13%. There is no reason[52] to expect f_{m}, the friction coefficient per particle opposing the motion of polymers moving en masse as in response to local concentration gradients, to be identical with the molecular friction factor, f_{s}. Nevertheless, both are at least expected to increase with concentration. So, there should be more resemblance than there is for D_{s} and D_{m}, which ordinarily diverge with concentration in good solvents. In any case, f_{m} can be obtained from eq 13 if D_{m} and $(\partial\pi/\partial c)_{T,p}$ are measured, and this is perhaps the maximum dynamic information that one can obtain from DLS measurements at small qL.

At large qL, and still in dilute solution, additional exponential decay terms appear in the correlation function representing local motions, especially rotation. For optically isotropic rigid rods, neglecting coupling of rotation and translation,

$$g^{(1)}(\tau) = S_0(qL)\exp(-D_{\mathrm{m}}q^2\tau) + S_1(qL)\exp(-D_{\mathrm{m}}q^2 - 6D_{\mathrm{r}})\tau + \dots \tag{14}$$

where D_{r} is the rotational diffusion rate. The amplitude S_1 becomes significant relative to S_0 at $qL > \approx 5$; for example, $S_1 \approx 0.1S_0$ at $qL = 5$. If the experimental data are sufficiently free of noise, a two-exponential fit will yield both D_{m} and D_{r}. The higher order terms will also

affect the average decay rate, $\bar{\Gamma}$, sometimes called the first cumulant:[53]

$$\bar{\Gamma} = \lim_{\tau \to 0} \left[\frac{d(g^{(1)}(\tau))}{d\tau} \right] / g^{(1)}(\tau) \quad (15)$$

The first cumulant increases as q^2 for pure translational motion and somewhat faster at high qL if rotational motion becomes important. There are several theories of the first cumulant of long rods in dilute solution;[54-56] the situation has been recently reviewed.[57,58] Perhaps the treatment of Schmidt and Stockmayer[54] gives the simplest expression:

$$\bar{\Gamma}/q^2 = D(1 + Cq^2R_g^2 + ...) \quad (16)$$

with $C = {}^1/_{30} = 0.033$ for rigid rods. Experiments on tobacco mosaic virus[55] seem to confirm this,[54] at least approximately, but until recently there was no extension to high concentrations.

(d) Dynamic Light Scattering in Concentrated Solutions. Using eqs 12, 13, and 15 for isotropic scattering, one easily obtains for the apparent diffusion coefficient

$$\bar{\Gamma}/q^2 = (k_BT/f_m)(1 + 8\nu/\nu^*) \quad (17)$$

The incompleteness of eq 17 is immediately evident, for it cannot account for the increase of $\bar{\Gamma}/q^2$ with q^2 at low concentration as eqs 14 and 16 do in the case of dilute solutions. DSO wrote a kinetic expression valid for a single rod and then extended it by application of the fluctuation–dissipation theorem to obtain the dynamic structure factor for the entire ensemble of rods. The resulting eqs 3.24 and 3.25 of DSO-II can be expressed

$$\bar{\Gamma}/q^2 = (k_BT/f_m)(1 + 8\nu/\nu^*)(1 + B(\nu)(qL)^2) \quad (18)$$

where

$$B(\nu) = \frac{D_rL^2}{1080D_s} - \frac{D_\parallel - D_\perp}{135D_s} - \frac{2\nu/\nu^*}{9(1 + 8\nu/\nu^*)} \quad (19)$$

$D_\parallel$ and $D_\perp$ are (self) diffusivities parallel to and perpendicular to the rod at the concentration ν. DSO actually used D_s in place of k_BT/f_m. It is unclear whether or not this reflects a belief that f_m and f_s will be quantitatively similar, but we shall maintain the distinction. $B(\nu)$ is positive at small ν, as it must be to account for rotation:

$$B(\nu) = \frac{1}{36}\left[\frac{1}{10} - \frac{8\nu/\nu^*}{1 + 8\nu/\nu^*}\right] \quad (20)$$

As $R_g^2 = L^2/12$ for a rod, it is easily seen that this is completely consistent with eq 16 in the limit of infinite dilution. However, the new result is that $B(\nu)$ decreases with ν. The original Doi and Edwards (DE) theory[59,60] made the assumptions $D_\parallel = D_\parallel^\circ = 3D^\circ/2$ and $D_\perp = 0$ in the semidilute regime. The superscript "°" represents the dilute solution limit. The principal DE result is that rotational diffusion is severely restricted: $D_r \propto D_r^\circ(\nu L^3)^{-2}$. If correct, then at high concentrations where $D_rL^2 \ll D_s$

$$B(\nu) = -\frac{1}{9}\left[\frac{1}{5} + \frac{2\nu/\nu^*}{1 + 8\nu/\nu^*}\right] \quad (21)$$

Thus, $B(\nu)$ can become negative, a result that was observed previously,[19] but not understood prior to the DSO theory. Qualitatively, this reflects that the motions responsible for relaxing the correlation function at high qL are not subject to long-range driving forces such as $(\partial\pi/\partial c)_{T,p}$ measured in the low-q macroscopic limit. In his matrix reformulation[61,62] of the DSO theory, Maeda introduced a length-dependent osmotic virial coefficient, $A(qL)$, to account for the shift from the macroscopic properties that SLS and DLS observe at low qL to the more microscopic viewpoint at high qL.

The correlation functions contain information beyond the first cumulant. Maeda's numerical extension of the DSO theory enables $g^{(1)}(\tau)$ to be calculated at arbitrary qL and ν. The computed correlation functions are decidedly nonexponential, and, in principle, one could vary parameters such as D_r to obtain agreement with the measurements. Very slow decay modes not predicted by the random phase formalism make this difficult. Also, before submitting to numerical analysis, one might first wish to validate the basic tenets of the theory, as given in DSO-III, where $g^{(1)}(\tau)$ is predicted to be biexponential. The physical insight into the two-mode prediction will be discussed in connection with the actually observed decay spectrum in section V.

III. Materials and Methods

Details appear in the supplementary material and may be of some interest to others working with this system or any concentrated polymer solution in a polar, hygroscopic solvent. Briefly, five samples of PBLG purchased from Sigma were fractionated from DMF by very slow vapor sorption of the nonsolvent methanol. The DMF used throughout this work was Aldrich "Gold Label" DMF containing <0.005% water. Distillation, filtration, and centrifugation were combined to reduce "dust" from solvent, polymer, and glassware while simultaneously preventing water contamination of the very hygroscopic solvent and solutions. The final samples were flame-sealed under a dry nitrogen atmosphere at reduced pressure. Specific refractive index increments were determined for unfractionated PBLG-260 000 at 25 ± 0.05 °C using a modified Brice-Phoenix differential refractometer. The results, in units of mL/g, are $dn/dc = 0.118 \pm 0.004$ (632.8 nm), 0.124 ± 0.002 (589 nm), 0.124 ± 0.003 (514.5 nm), and 0.127 ± 0.002 (488 nm).

Most measurements were made in the Uv geometry (vertically polarized incident beam; unpolarized detection) on a goniometer described elsewhere.[63,64] For most samples this is virtually indistinguishable from the Vv scattering geometry (vertically polarized incident beam; vertically polarized detector). All static measurements were made with relatively incoherent detector optics using an incident wavelength of 514.5 nm, where the Uv Rayleigh factor for the toluene reference is 3.208×10^{-5} cm^{-1}.[65,66] The optical coherence of the detector was increased for dynamic light scattering, and λ_0 was changed to 488 nm to achieve higher q values so that eqs 16–21 could be tested. All measurements were made in the homodyne mode,[48] where, assuming Gaussian fluctuations, the measured intensity autocorrelation function $G^{(2)}(\tau) = B(1 + f|g^{(1)}(\tau)|^2)$. Here B is the baseline and f is an instrumental parameter ($0 < f < 1$) depending mostly on optical coherence. The channel time of the correlator was set to ensure complete decay of the measured correlation function, within instrumental limitations. It was possible to expand greatly the display scale of the 272-channel Langley-Ford Model 1096 correlator to test very carefully for a flat baseline. In concentrated solutions, this revealed very slow decay modes, and an attempt was made to measure the full correlation function using the "multi-τ" mode of the correlator, with an "expander" of 16. In this mode, the instrument collected three correlation functions simultaneously using precisely the same data stream, but at different sample times (the shift register configuration is automatically adjusted to prevent overflows). The first function contained 48 channels separated by the "base" sample time, $\Delta\tau$; the second, 64 channels separated by $16\Delta\tau$; the third, 32 channels with a separation of $16^2\Delta\tau = 256\Delta\tau$. Thus, the total time "window" had a width of $32 \times 256\Delta\tau = 8192\Delta\tau$. At high concentrations, even this was insufficient.

A given correlogram was collected as a series of about 10 short runs, each of which was analyzed for consistency of intensity, decay rate from a second-order cumulants fit,[53] degree of nonexponentiality, correlation of residual errors from channel to channel, and weighted residuals of fit, χ^2.[67] An additional quality

Table I
Characteristic Parameters of the Four PBLG Fractions

$M^a/10^3$	$x = L/d^b$	νdL^2 at $\nu/\nu^* = 1^c$	νL^3 at $\nu/\nu^* = 1^c$	$c/(g\ mL^{-1})$ at $\nu/\nu^* = 1^c$	$c/(g\ mL^{-1})$ at Flory A point^d	max value of ν/ν^* measd
277	119	5.3	624	0.0425	0.083	2.17
179	77	4.7	359	0.0573	0.128	1.35
149	63	4.4	280	0.0655	0.149	1.07
60	26	3.3	85	0.122	0.359	1.31

[a] The determination of the average value of M is described in Table II. [b] The length was computed according to eq 4; d = 1.6 nm. [c] $\nu^* = 4/A_2{}'$, where $A_2{}'$ is obtained from the average over all temperatures for a given molecular weight (Table II). [d] The volume fraction at the Flory A point was calculated as $\phi_A = (8/x)(1 - 2/x)$, where $x = L/d$, with L taken from eq 4 and d taken as 1.6 nm (see text). The conversion to concentration used the partial specific volume, 0.791 cm^3/g.[76]

parameter was the agreement between the theoretical baseline, $B_t = P(P-O)/N$, where P is the number of photopulses detected, O the number of shift register overflows, and N the number of sample times (typically, 10^7, 0, and 10^7, respectively). The consistency among the short runs was generally very good, and most were retained and summed together to generate a correlogram for further data analysis and plotting. Algorithms applied to the summed data included the following: 1st–3rd cumulants, 1CUMU–3CUMU; nonlinear least-squares multiple exponential, m-EXP, where m is an integer; smoothed exponential sampling,[68,69] EXSAMP; and Provencher's CONTIN.[70] The cumulant analyses always used baseline B_t, and this was quite common in the other methods, except at the highest concentrations. It was also possible to fit a baseline, B_f. A useful parameter is the "liftoff", defined as the difference between the fitted baseline from a multiple exponential fit to $G^{(2)}(\tau)$ with floated baseline and B_t, normalized by baseline uncertainty: liftoff = $(B_{f,m\text{-EXP}} - B_t)/\sigma_B$, where σ_B is the baseline uncertainty, $B_t^{1/2}$, and m is the integer number of exponentials in the fit. The liftoff is usually positive, because a multiple-exponential algorithm with floating baseline attempts to mask any slow decay as baseline. When characterizing polymers in dilute solution, liftoffs > 10 when $m = 3$ usually indicate some sort of pathological behavior, such as dust or number fluctuations.[48] For $N \approx P \approx 10^7$, this criterion corresponds to $B_{f,m\text{-EXP}} \approx 1.003B_t$. During the course of the present work, larger liftoffs were observed at high concentrations, due to slow modes that could not be traced to sample preparation problems. All but the first few channels available from the correlator were fitted, with two important exceptions. In the cumulants analysis, channels for which the uncertainty exceeded 33% of the signal after baseline subtraction were not used. Also, for "multi-τ" measurements at high concentrations the 3CUMU values were taken from just the first 48-channel correlation function measured at the base sample time. This effectively isolated the initial decay rate.

IV. Static Light Scattering Results and Discussion

(a) General Remarks. To facilitate discussion, Table I lists conversion factors that allow the critical concentration ν^* to be understood in more conventional terms, such as c, the Flory A point, and number densities relative to L^3 or dL^2. Other molecular parameters also appear. In this table, ν^* at a given molecular weight is determined using the *average* value of A_2 at all measured temperatures. Elsewhere, whenever ν^* is used, it is derived from virial coefficient measurements at a specific indicated temperature and molecular weight. In fact, no virial coefficient differs very much from the average; still, the purpose of Table I is only to provide a qualitative sense of the various concentrations.

(b) Static Light Scattering in Dilute Solution. Molecular parameters extracted from Zimm plots at low concentration appear in Tables II and III. The averaged radii of gyration are in excellent agreement with those expected from eqs 3 and 4, where the measured molecular weights have been used. Not surprisingly, the largest deviation occurs at the lowest molecular weight where the measurements are least accurate and least precise. Even

Table II
Virial Coefficients at Various Molecular Weights and Temperatures

	$A_2/(10^{-4}$ cm^3 mol g$^{-2})$			
T/°C	M^a = 277 000	M = 179 000	M = 149 000	M = 60 000
5		3.52		
15		4.14	3.94	5.36
20		4.43		
25		5.46		
30	3.35			
40		3.86	3.35	5.38
75	3.45	3.80	4.77	5.70
av	3.40 ± 0.10	4.28 ± 0.66	4.02 ± 0.71	5.48 ± 0.19

global (total) average = (4.35 ± 0.83) × 10^{-4} cm^3 mol g^{-2}
average (excluding M = 60 000) = (3.9 ± 0.45) × 10^{-4} cm^3 mol g^{-2}

[a] Molecular weights are averaged over temperature. The variance is 5–10%.

so, the measured result is almost within error of the value calculated for a thin rigid rod. The average linear mass density, computed in the rodlike limit as $M/12^{1/2}R_g$, is (1.33 ± 0.12) × 10^{10} g cm^{-1} mol^{-1} when averaged over all four molecular weights. It is tempting to exclude the data for PBLG-60 000 on the grounds that measurement of R_g becomes inaccurate for smaller particles. For truly accurate measurements, R_g should exceed $\lambda_0/20n$, or 18 nm for the present case (λ_0 = 514.5 nm and n = 1.43). However, past experience suggests that our apparatus maintains reasonable accuracy at or even below the 12-nm size of PBLG-60 000. The real reason for difficulties at M = 60 000 appears to be the greater polydispersity of this fraction. Neglecting PBLG-60 000, the linear mass density is (1.39 ± 0.02) × 10^{10} g cm^{-1} mol^{-1}—just 5% lower than the expected value for a rigid α-helix. The corresponding apparent translation per monomer unit is 0.158 ± 0.003 nm. The difference compared to h_α is attributable to the residual mass heterogeneity. It is possible to estimate the severity of the polydispersity. The proportionality $(R_g^2)_z \propto M_zM_{z+1}$ for rods,[71] together with eqs 3 and 4, implies that $M_zM_{z+1}/M_w^2 = 12(R_g^2)_zM_0^2/(h_\alpha M_w)$.[2] All the experimental values (Table III) of this somewhat unusual polydispersity parameter are much lower than expected for a most probable distribution (M_zM_{z+1}/M_w^2 = 3). Only for PBLG-60 000 is the result distinguishable from unity, given realistic uncertainties. This implies that the polymers are reasonably homogeneous, the only caveat being that small amounts of low-M material would not appear in this analysis.

The measured virial coefficients are strongly positive at all temperatures; see Table II. We were unable to verify the report[72] that $A_2 = 0$ at about 23 °C. Instead, the data confirm the negligible temperature dependence reported by Kubo and Ogino.[73] The most likely explanation for the wrong claim that $A_2 = 0$ at 23 °C is minor water contamination; PBLG/DMF solutions are highly sensitive even to very small amounts of water.[74] This has actually

Table III
Radii of Gyration for Various Molecular Weights[a] Averaged over Temperature

	M = 277 000	M = 179 000	M = 149 000	M = 60 000
$R_g/(10^{-6}$ cm)	5.64 ± 0.56	3.77 ± 0.36	3.10 ± 0.05	1.51 ± 0.24
$R_{g,calc}$[b]$/(10^{-6}$ cm)	5.48	3.54	2.95	1.19
% diff	3	5	5	27
$(M/12^{1/2}R_g)$[c]$/(10^{10}$ g cm^{-1} mol^{-1})	1.42	1.37	1.39	1.15
$12(R_g^2)_z M_0^2/h_\alpha^2 M_w^2 \equiv M_{z+1}M_z/M_w^2$	1.06	1.13	1.11	1.62

[a] Molecular weights and radii are averaged over the temperatures used. The uncertainty quoted for R_g of any given sample is the square root of the sample variance over measurements at different temperatures. [b] See eqs 3 and 4. [c] Global average = (1.33 ± 0.12) × 10^{10} g cm^{-1} mol^{-1}; average (excluding M = 60 000) = (1.39 ± 0.02) × 10^{10} g cm^{-1} mol^{-1}; theoretical value for PBLG α-helix = 1.46 × 10^{10} g cm^{-1} mol^{-1}.

led to the assertion[75] that the PBLG/DMF system is an inappropriate model of rodlike polymers. In fact, when care is taken to keep the solvent and solutions dry, hardly any system could be more ideal. Uncertainties assigned to the virial coefficients based on standard propagation of the errors in the raw intensity measurements are only about ±5%. Systematic errors (stray light, undulations and scratches on cells, concentration errors, etc.) are undoubtedly larger. Thus, there is probably no significant trend to the data, with the exception that A_2 may increase slightly with decreasing M, in agreement with Kubo and Ogino.[73] Excluding the PBLG-60 000 fraction, the average is A_2 = (3.90 ± 0.45) × 10^{-4} cm^3 mol g^{-2}. Solving eq 5 for d using the experimental linear mass density from R_g and M_w measurements (again, excluding the PBLG-60 000 data) yields d = 1.60 ± 0.12 nm. This is in excellent agreement with the diameter, 1.56 nm, of a smooth cylinder with density equal to the inverse of the partial specific volume of PBLG in DMF (0.791 mL/g[76]) and the theoretical linear mass density of 1.46 × 10^{10} g cm^{-1} mol^{-1}. Recently, the *cross-sectional* radius of gyration for PBLG was found by deuterium NMR experiments[77] in the liquid crystalline phase to be 0.65 nm. The diameter of a solid disk having this cross-sectional radius of gyration would be 0.65 × $2^{3/2}$, or 1.84 nm—just 14% higher than the experimental or smooth-cylinder values.

These considerations suggest that treating the solvent as a continuum and the polymer as a smooth cylinder is reasonably well justified in a thermodynamic sense for PBLG/DMF. Ironically, the validation for this Onsager-type viewpoint may be supplied by PBLG's flexible side chains—specifically, by their dynamic nature. If two perfectly smooth rods immersed in a solvent of finite size are made to touch, some solvent is excluded from the junction zone. The resultant imbalance of random forces upon the rods pushes them together, thereby reducing the apparent virial coefficient. This cannot happen for "point solvents"—hence the Flory–Ronca argument[7] that cluster expansion theories must always overestimate A_2 (and therefore underestimate the critical point). However, if the rods have flexible side chains, then a combination of side chain libration and rapid rotation of the rods about their long axes restores the randomness of force exerted on the backbone in the vicinity of the junction.

(c) Static Light Scattering at Higher Concentrations. The results so far indicate that experimental inaccuracies, finite thickness effects, finite solvent size, polydispersity, and flexibility are all essentially negligible *in dilute solution*. Perhaps some of these effects, particularly flexibility,[78] will be more obvious at higher concentrations. Osmotic moduli—suitably normalized for temperature and molecular weight—are plotted against ν/ν^* in Figure 1. No adjustable parameters were used to assemble this plot; ν^* was calculated from the value of A_2 measured at each temperature and molecular weight. The molecular weights are averages over the temperatures at which measurements were made, but this is of no consequence as the values are virtually identical at all temperatures, within error. Thus, the observed scaling behavior is very satisfying. The data well represent the Onsager expectation, $(\partial\pi/\partial c)_{T,p}\, M/RT = 1 + 8\nu/\nu^*$. At $\nu/\nu^* < 1$ the slope of the line through all the data points is 6.86 ± 0.55, only about 14% low. There is a relationship between this deviation and the 14% difference between the diameter obtained from A_2 and that from NMR: $A_{2,\nu}$ is proportional to d.

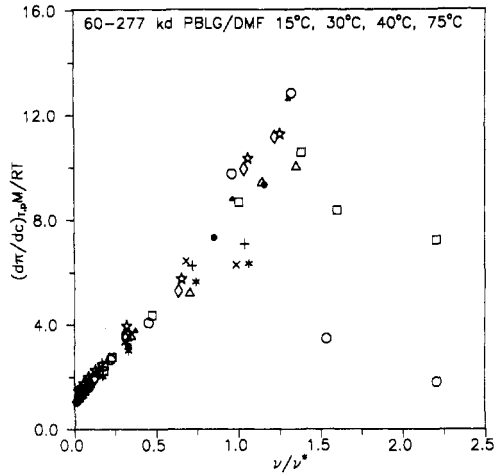

Figure 1. Scaled osmotic moduli for all temperatures and molecular weights. No adjustable parameters are used to assemble this plot. Symbols: (○) 277 000 g/mol at 30 °C; (□) 277 000 g/mol at 75 °C; (△) 179 000 g/mol at 15 °C; (◇) 179 000 g/mol at 40 °C; (☆) 179 000 g/mol at 75 °C; (+) 149 000 g/mol at 15 °C; (×) 149 000 g/mol at 40 °C; (*) 149 000 g/mol at 75 °C; (●) 60 000 g/mol at 15 °C; (▲) 75 °C. Estimated errors: 5–10%.

An equilibrium nematic phase occurs at ≈17.5 wt % ($\nu/\nu^* \approx 4$, $\phi \approx 0.14$) for PBLG-277 000 at room temperature,[79] in good agreement with the phase diagram of Miller and co-workers for a PBLG of similar molecular weight.[80] Downward deviations in osmotic modulus begin at $\nu/\nu^* \approx$ $^3/_2$ for this largest polymer fraction. As discussed in section IIa, this is a natural consequence of coupled alignment/concentration fluctuations as the nematic is approached. In contrast to dilute solution, flexibility effects are visible. For example, the downturns in osmotic modulus are forestalled by raising the temperature. This is probably because temperature-induced flexibility shifts the nematic transition to higher concentrations in PBLG/DMF,[80] reducing the magnitude of alignment fluctuations and coupled concentration effects.

Despite the discussion in section IIa, some might be tempted to describe the downturns in osmotic modulus as "aggregation", based on experience with random coil solutions, which ordinarily do not undergo liquid–liquid phase separation in good solvents. We emphasize that A_2 is very close to the excluded volume value and seems quite adequate up until ≈ν^*. Even at the highest measured concentrations, $(\partial\pi/\partial c)_{T,p}$ remains positive. PBLG/DMF is known to form a lyotropic phase in which the rods remain

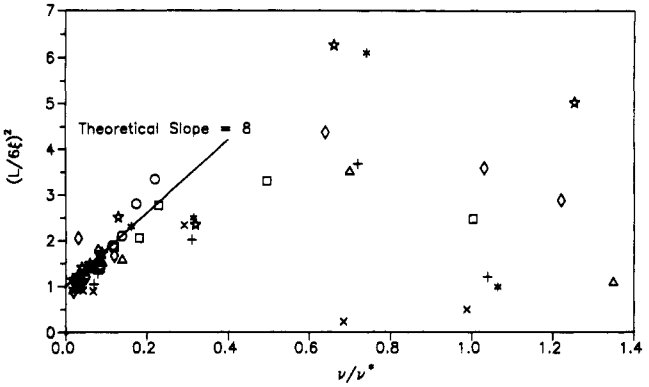

Figure 2. Correlation length, scaled by molecular length, plotted as suggested by eq 10. A line with the theoretical slope of 8 and unit intercept is shown. Data at high concentrations for PBLG-277 000 are not shown. Symbols as in Figure 1.

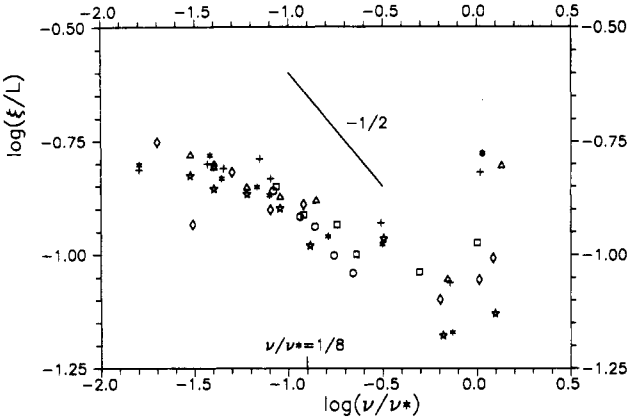

Figure 3. Correlation lengths, scaled by molecular length, plotted as suggested by eq 11. A line of $-1/2$ slope is displayed for reference. The very large correlation lengths observed for PBLG-277 000 at high concentration are not shown. Symbols as in Figure 1.

molecularly dispersed.[74,81] All this argues against aggregation, at least in the usual sense of random coalescence of molecules caused by unfavorable polymer–solvent energetics. The depolarized results below will reinforce the role of alignment in reducing the osmotic modulus.

None of the data extend to the limit of instability, $(\partial\pi/\partial c)_{T,p} = 0$. When observed between crossed polars in microscope, even the most concentrated samples failed to show any sign of the cholesteric phase. Kubo and Ogino, who measured osmotic pressures on both sides of the nematic transition in PBLG/DMF,[73] found a somewhat delayed onset of the nematic transition, especially at high M. They also did not see any well-defined region where $(\partial\pi/\partial c)_{T,p} = 0$, blaming this on flexibility. Similar observations have been made in other systems.[82]

The concentration dependence of the correlation length is shown in Figure 2. Clearly, the data do exhibit the behavior described by eq 10 up to $\nu/\nu^* \approx 0.2$, with a measured slope near the predicted 8. At slightly higher concentrations, ξ is sufficiently small that its accurate measurement with visible light becomes difficult, so the data are noisy. Nonetheless, it is evident that the quantity $(L/6\xi)^2$ does not maintain its increase at higher concentrations; ξ decreases less rapidly than predicted.

To understand the downward curvature of Figure 2, first it is necessary to consider the accuracy with which ξ can be measured. Equation 9 may be rewritten

$$\frac{g(0)/g(q) - 1}{q^2} = \xi^2 + \mathcal{D}q^2 + \ldots = \xi_{app}{}^2 \qquad (22)$$

The true value of ξ can be obtained only in the limit of "small" q. How small depends on the concentration, as $\mathcal{D}$ is a function of c. Initially, its sign is positive and its magnitude small, so that ξ is slightly overestimated from data at finite q. That is, the apparent correlation length is slightly larger than the actual. It is possible to estimate the magnitude of the error from eqs 8 and 22. At $\nu/\nu^* = 0.2$ for $L = 200$ nm, assuming a scattering angle of 60° (chosen to represent about the average angle from which the correlation lengths were determined), $\lambda_0 = 514.5$ nm, and $n = 1.43$, the error in ξ^2 is about 4%. At $\nu/\nu^* = {}^7/_{27} \approx 0.26$, the sign of $\mathcal{D}$ changes, after which its magnitude continues to increase. Now ξ will be underestimated—and the errors will become very serious as ν^* is approached. Nevertheless, at $\nu/\nu^* = 0.5$, $\mathcal{D}$ is only $-8 \times 10^{-5}L^4$. Thus, if $L = 200$ nm, one expects from eq 10 that $\xi^2 = (200)^2/(5 \times 36) = 222$ nm^2 ($\xi = 15$ nm), whereas the measurement under the scattering conditions just stated will only be 183 nm^2 ($\xi = 13.7$ nm), corresponding to an 8% error. The analysis can be repeated using Maeda's general numerical formulation of the DSO theory,[61,62] but the conclusion is the same: errors due to making the measurement at finite angles remain too small to account for the downturn in Figure 2. Moreover, the errors have the wrong sign at $\nu/\nu^* > {}^7/_{27}$.

Figure 3 facilitates the scaling analysis. The data at $\nu < \nu^*$ suggest an exponent with magnitude somewhat less than the predicted $^1/_2$. As ξ should decrease even faster for a random coil polymer than for a rod ($\xi_{coil} \propto c^{-3/4}$ [40,43]), it seems hard at first to blame the discrepancy on PBLG flexibility. However, it is possible to imagine that semiflexible molecules might actually straighten with concentration. The data would be consistent with this notion, except that the R_g's in dilute solution are so near the rigid, fully extended limit. The more likely explanation for a low exponent, and the downturn in Figure 2, is long-range correlations associated with the nematic transition, but not included in the theory. These are plainly evident as ν^* is approached and ξ again enters a size regime accessible to visible light but then quickly grows to a size that would require small angles of measurement beyond the scope of the present study.

It is interesting that the correlation lengths deviate from expectations at comparatively low concentrations while the osmotic moduli are well behaved to concentrations slightly beyond ν^*. As stated earlier, even though the DSO model treats the spinodal character of isotropic–nematic transition, it is primarily intended for systems not too far from equilibrium, much the same as linear classical Cahn–Hilliard theory is for simple fluids.[83] We speculate that ξ may be more sensitive to the limitations of the mean field approximations than $(\partial\pi/\partial c)_{T,p}$.

(d) Depolarized Measurements. The α-helical structure of PBLG results in a polarizability tensor that is far more isotropic than one might suspect from the overall rodlike shape. In dilute solution it is actually quite difficult to measure the depolarized intensity above that scattered by the polar solvent. This is quite unlike rodlike polymers with rigid backbones, such as poly(p-phenylenebenzobisthiazole).[84] Thus, in Uv scattering experiments on PBLG/DMF, orientational effects will only appear indirectly via coupling to concentration fluctuations. Fortunately, the polarizability tensor of PBLG is not completely isotropic; difficult experiments in the Hv geometry (vertically polarized incident beam; detection of only horizontally polarized light) are directly sensitized to the orientational behavior.

Let δ_0 be the intrinsic optical anisotropy of the perfectly rigid molecules, which one could measure by extrapolation

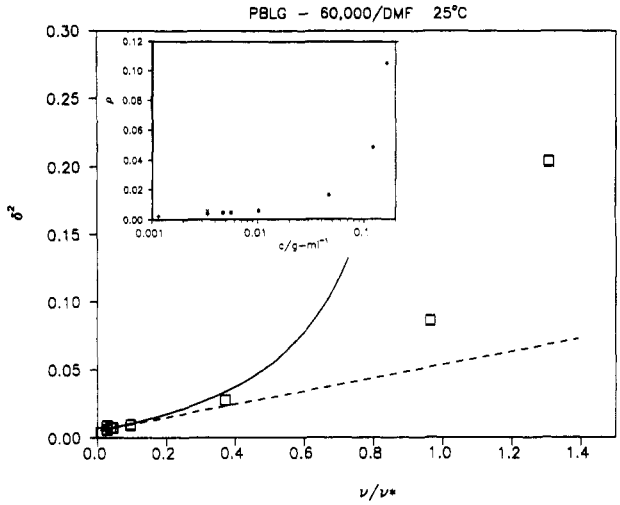

Figure 4. Apparent optical anisotropy increases with concentration for PBLG-60 000 at 25 °C. Dashed line: least-squares fit through data at $\nu/\nu^* < 0.2$ (best fit results appear in text). Solid curve predicted by Maeda; see eq 24. Inset: Depolarization ratio at $\theta = 45°$ from which δ is derived. Except at lowest concentration, duplicate measurements are plotted (error is comparable to symbol size).

to infinite dilution. For molecules of cylindrical symmetry, $\delta_0 = (\alpha_\parallel - \alpha_\perp)/(\alpha_\parallel + 2\alpha_\perp)$, where $\alpha_\parallel$ and $\alpha_\perp$ are polarizabilities parallel and perpendicular to the molecular axis. The apparent optical anisotropy, δ, at arbitrary concentration can be determined from the depolarization ratio, $\rho = g_{Hv}/g_{Vv} = 3\delta^2/(5 + 4\delta^2)$. Ideally, depolarization ratios at all molecular weights and concentrations would be extrapolated to $\theta = 0$. But due to the weak depolarization, we only studied the concentration effect for PBLG-60 000 at just one moderately low angle ($\theta = 45°$). However, it was ascertained that an ≈8% solution of PBLG-277 000 (among the most concentrated, relative to ν^*) exhibited just-moderate angular dependence, at least for $\theta > 30°$. Apparent optical anisotropies for PBLG-60 000 are shown in Figure 4. Increases representing enhanced molecular alignment are evident.

Benoit and Stockmayer[85] were the first to treat depolarized scattering from rods at high densities. Their theory is limited to cases in which intermolecular forces are relatively short range and molecular size does not approach the wavelength of light. The latter condition is not true for any of our fractions but is most closely approximated by PBLG-60 000. A specific prediction is reached for the concentration dependence of δ:

$$\delta^2/\delta_0^2 = 1 + 9\nu/\nu^* \tag{23}$$

This expression is obtained by combining eqs 2.9 and 2.10 of ref 85 with eq 6 herein. Maeda's numerical extension of the DSO approach[61,62] treats the Hv scattering geometry. In the limit of relatively low angles and concentrations the predicted depolarization ratio is[62]

$$\rho = (1 - \nu/\nu^*)^{-1}/(1 + 8\nu/\nu^*)^{-1} = (1 + 8\nu/\nu^*)/(1 - \nu/\nu^*) \tag{24}$$

Considering that δ is usually quite small, eqs 23 and 24 are clearly identical at small ν.

A linear least-squares fit (dotted line) to the data in Figure 4 at $\nu/\nu^* < 0.2$ yields $\delta_0^2 = 0.00535 \pm 0.0008$. Dividing this into the poorly determined slope gives 9 ± 3, to be compared with the predicted 9 of eqs 23 and 24. The linear correlation coefficient is a very low 0.78, so the agreement can only be described as qualitative. Nevertheless, the result is acceptable given the difficulty of depolarized experiments at low concentration in this system. Agreement with the Benoit–Stockmayer theory is fully consistent with polarized scattering results that confirm the Onsager or DSO predictions; the essential ingredient in all these theories is careful treatment of excluded volume. At higher concentrations the amount of light depolarized increases strongly. A rapid rise in depolarized scattering indicates progressively more pronounced orientation fluctuations that presage the stable nematic phase. The solid curve shows the prediction of eq 24. In keeping with previous observations (e.g., Figure 1), ν exceeds ν^* without any evident transition. Nevertheless, the large increase in δ makes it plausible that even relatively weak orientation–concentration coupling can become easily observable in the polarized scattering. It is also clear that local orientational order is enhanced compared to infinitely dilute solution at remarkably low concentrations—very far from the lyotropic boundary. The forces that ultimately lead to the nematic phase are evident much earlier. This is not too surprising; Table I shows that $\nu/\nu^* = 0.1$, by which concentration the increase in δ^2 in Figure 4 is undeniable, corresponds to $\nu L^3 \approx 8.5$ for PBLG-60 000. Cramming over 8 rods into a box with volume equal to the cube of their length *should* produce serious interactions. It must be remembered that the interactions produce only fluctuations in the single-phase regime. The reports[86] of "pretransitional phenomena" in solutions of rodlike polymers held just below the nematic concentration suggest, however, that such fluctuations may be very long-lived. The dynamic behavior of concentration and coupled orientation fluctuations is the subject of the remainder of this paper.

V. Dynamic Light Scattering Results and Discussion

(a) Simple Cumulants Analysis of Polarized Scattering. The correlation functions were nearly single-exponential decays at low angles and low concentrations but, in general, nonexponential character was evident. In most cases it was simple to extract $\bar{\Gamma}$. For example, a third-order linear least-squares fit to the linearized correlation function was often adequate: $\ln (G^{(2)}(\tau) - B_t)^{1/2} = \text{intercept} - \bar{\Gamma}\tau + \mu_2\tau^2 - \mu_3\tau^3$, where $\mu_2/\bar{\Gamma}^2 = 0$ for a single-exponential decay. The average decay rate so obtained can be compared to that from a nonlinear fit of $G^{(2)}$ to a single exponential with floating baseline: $G^{(2)}(\tau) = B_{f,1EXP}(1 + f\exp(-2\bar{\Gamma}\tau))$. For many samples, these two estimates of $\bar{\Gamma}$ were in good agreement. In sections Vb–d, the effects and significance of nonexponentiality are discussed in detail, but much can be learned just from the average decay rates.

Figure 5 shows the dependence of $\bar{\Gamma}$ on q^2 for PBLG-277 000 at 30 °C. At a relatively low concentration, 0.00494 g/mL, $\bar{\Gamma}$ scales linearly with q^2 at low q, but an upward curvature is evident at higher q, as expected (see eqs 14 and 16). At 12 times the concentration, the curvature is downward, consistent with the DSO predictions (see eqs 19–21). The same effects were evident at 75 °C for this fraction, but the downward curvature was somewhat suppressed.[87] Recall that the downturn of the osmotic modulus with concentration is also suppressed by raising the temperature. Both effects are associated with proximity to the nematic transition, which shifts to higher concentrations with increased temperature due to enhanced flexibility.[9,80] PBLG-179 000 and PBLG-149 000 also exhibited downward curvature of $\bar{\Gamma}$ vs q^2 at high concentrations and various temperatures. Upward curvature at low concentration was considerably less pro-

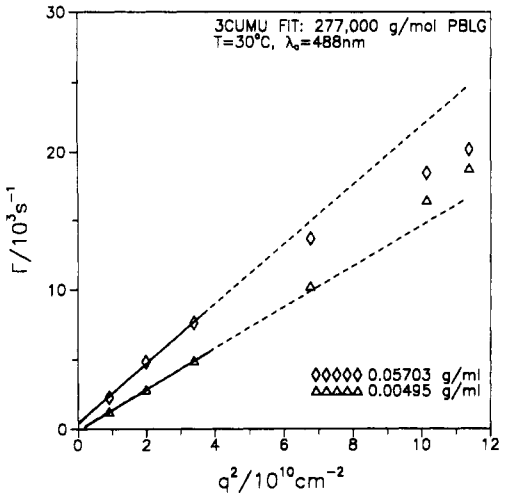

Figure 5. 3CUMU decay rates are plotted against q^2 for PBLG-277 000. Upward curvature at low concentrations gives way to downward curvature at higher concentrations. See text. Estimated errors: 3–5%.

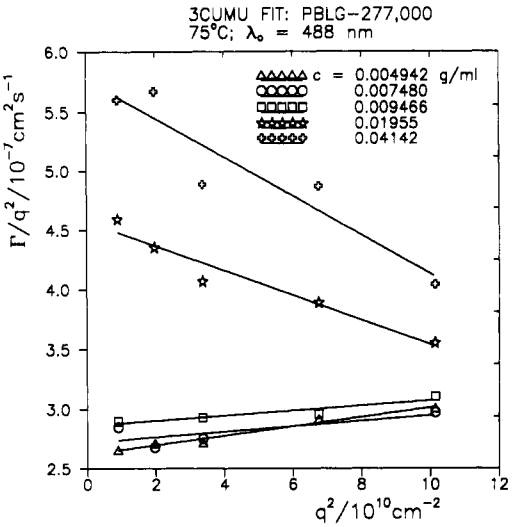

Figure 6. Apparent diffusivity Γ/q^2 vs q^2 for PBLG-277 000 at 75 °C for several concentrations (in g/mL): (△) 0.00494; (○) 0.00748; (□) 0.00947; (☆) 0.0196; (+) 0.0414. See also Figure 5.

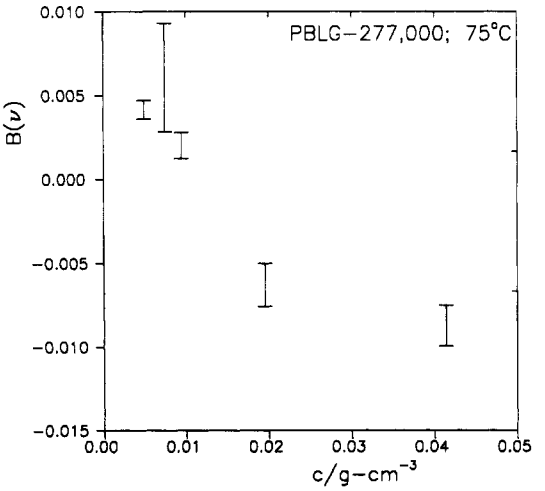

Figure 7. Slope of lines in Figure 6, indicating that $B(\nu)$ changes sign from positive to negative, see text.

nounced, as expected given the lower qL values (the maximum value of qL for PBLG-179 000 was only about 4). PBLG-60 000, despite its very short length, exhibited positive curvature in dilute solution. In this case, polydispersity—not rotation—is responsible; nonuniform molecules of finite size exhibit positive curvature because the scattering from large particles is deemphasized at higher scattering angles due to intramolecular interference. This eliminates aggregation—at least of a type leading to a broader distribution of scattering size—as the cause of downward curvatures at high c. Like the larger fractions, enhanced concentration of PBLG-60 000 reduced the positive curvature and the plots became essentially linear.

Reduction of downward curvature with temperature is a particularly intriguing observation. If the first cumulant is sensitive to relatively modest temperature-induced changes in polymer flexibility, then perhaps this can be exploited. Considerable effort has gone into development of theories that enable persistence length to be measured from the q dependence in dilute solution (for an entry to the literature, see refs 57 and 58). For long filaments, persistence lengths have been accurately measured even in the stiff limit, $L/a < 1$.[88,89] However, it remains difficult to measure the persistence length of a *short*, stiff polymer by dynamic light scattering in dilute solution. Perhaps with proper theoretical development, one could obtain a from the $\bar{\Gamma}$ vs q^2 behavior of a single, moderately concentrated solution. Repeat measurements at different temperatures would be trivial. A word of caution is in order.[58] Some theories already claim to treat semiflexible polymers in the semidilute limit. This refers only to simple assumptions about the anisotropic nature of the diffusion process. To our knowledge, no theory correctly takes excluded volume, flexibility, and anisotropic mobility into consideration. Still, the persistence length of short, stiff filaments is a recurring problem, and an appropriate theory to take advantage of the apparent sensitivity of the first cumulant at high concentrations would be a valuable asset.

The slopes in Figure 6 give $B(\nu)$, which is plotted against concentration in Figure 7. The crossover from positive to negative $B(\nu)$ occurs at $\approx$0.01 g/mL ($\nu/\nu^* \approx 1/4$) for PBLG-277 000. The slope of Figure 6 at the lowest concentration can be combined with the measured R_g to obtain the parameter C in eq 16. The resulting value is at least 30% higher than the predicted 0.033. Even this is substantially lower than the value obtained in Schmidt's study of PBLG/DMF, perhaps due to differences in the molecular weight distribution or even details of how the first cumulant is isolated. In the absence of an independent molecular weight distribution, there is little point to trying to improve on the value of C or use it[18,54] to estimate persistence length.

Although the change in curvature with concentration is perhaps the most unusual feature of Figure 5, another important result is clearly visible: D_m increases with c. This behavior, already known for PBLG in DMF,[17-19] is another argument against aggregation. Parts a–d of Figure 8, showing D_m's determined from initial slopes of $\bar{\Gamma}$ vs q^2 plots, summarize the current results. Very rarely, a sudden downturn in D_m at high concentration was observed, as in Figure 8d. Absent completely from ref 19, but present in another study of PBLG/DMF,[17] the sudden downturns probably reflect proximity to the nematic; this, in turn, may depend on temperature. Downturns were also observed in aqueous xanthan.[90] Other studies of helical rods have found no clear trend in D_m, or various behavior depending on molecular weight and/or solvent conditions.[16,91]

Although the overall trend is increasing D_m with c for rods dispersed in a demonstrably good solvent, there is some evidence[19] that the very initial dependence of D_m on c is either level or slightly decreasing under these conditions. In the present study, the effect is most clearly seen

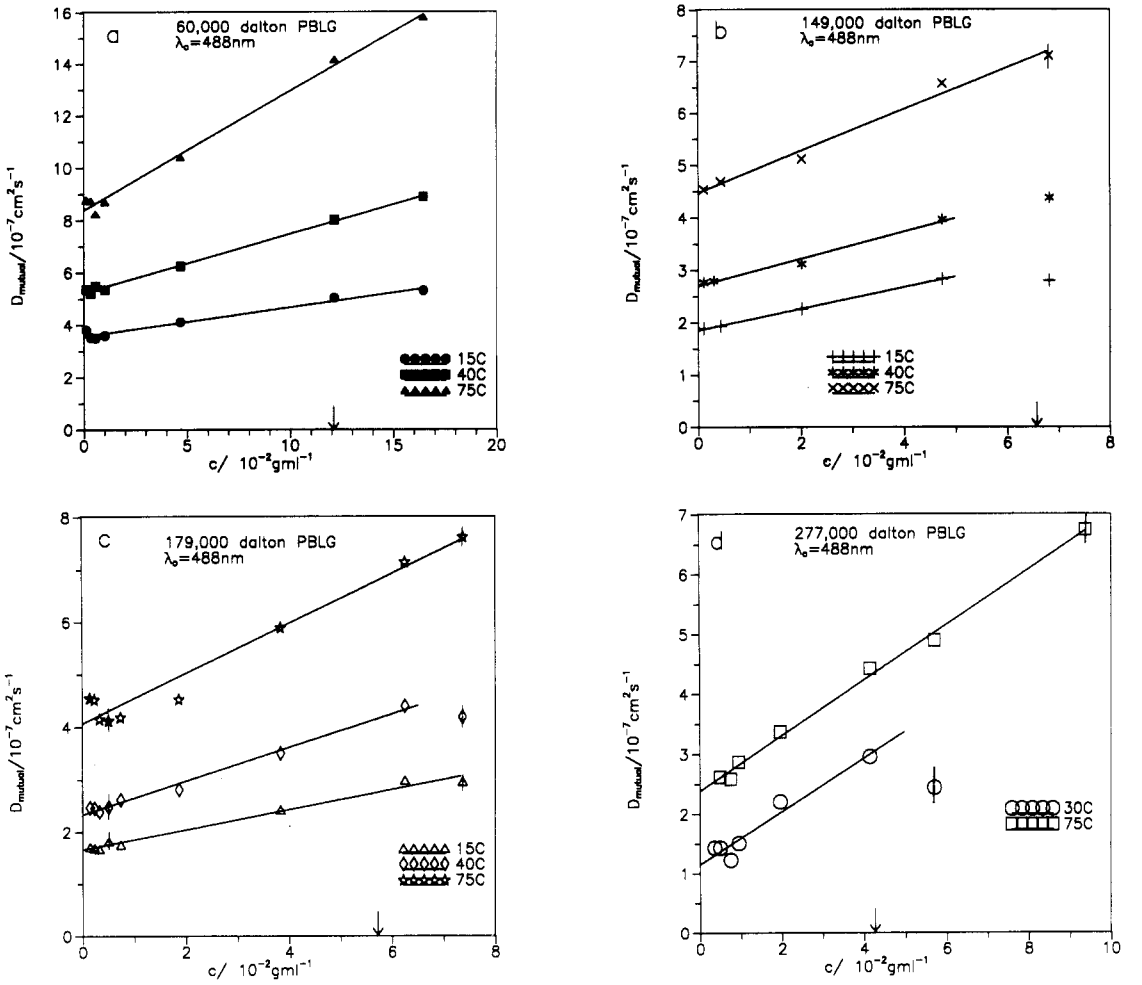

Figure 8. Concentration dependence of D_m for four PBLG fractions at various temperatures as indicated. The arrows show the concentration corresponding approximately to ν^*. Estimated error: smaller than point size, except where shown explicitly.

in Figure 8c, but is almost within experimental uncertainty. Others[92] have found a more clearly defined "shelf" near $c = 0$. It is both possible and instructive to rationalize this behavior. The measured D_m is the trace of a mobility tensor times a thermodynamic driving force; eq 17 may be rewritten $D_m \approx [(D_\parallel + 2D_\perp)(1 + 8\nu/\nu^*)]/3$. At low concentration, $D_m = D^\circ = {}^2/_3 D_\parallel^\circ$. Values at higher concentrations depend on what one assumes for the diffusion tensor components. In the classical Doi–Edwards model, one expects $D_m = [(D_\parallel^\circ + 2{\cdot}0)(1 + 8{\cdot}1)]/3 = 3D_\parallel^\circ$ at $\nu = \nu^*$—an increase by the factor ${}^9/_2$ over D°. The numerator represents the osmotic driving contribution, and the denominator the supposition that the inherent mobility will be reduced by half due to loss of lateral motion. Likewise, if the condition $D_\perp = 0$ is met at $\nu/\nu^* = {}^1/_8$, $D_m = D^\circ$ is predicted at this concentration. According to Figure 8, D_m at ν^* is 1.5–2 times larger than D° rather than the "expected" ${}^9/_2$. This probably invalidates the Doi–Edwards assumption that $D_\parallel$ is constant; the authors themselves admit the inaccuracy of this approximation.[44] Still, the above arguments demonstrate that, depending on the exact juxtaposition of thermodynamic driving forces and the decay of $D_\perp$ at a particular molecular weight, D_m could initially be a level or weakly decreasing function of c even in a good solvent.

Molecular weight, osmotic modulus, and D_m, all determined at low q, were combined to obtain f_m via eq 13. Figure 9 shows that f_m increases steadily with c and does not exhibit any sudden increases that could account for the occasional sharp downturns in D_m at high concentrations. According to eq 13, such downturns are therefore

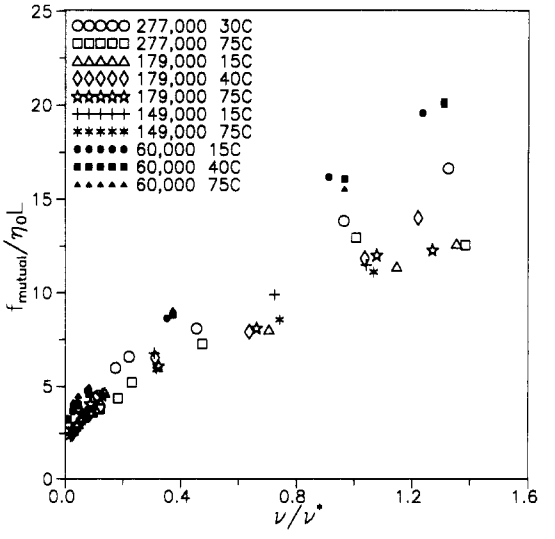

Figure 9. Mutual friction coefficient, scaled by solvent viscosity and rod length, at all measured conditions. Precision: ≈±15%; estimated accuracy: ≈±20%.

understood as the result of diminished osmotic modulus in the immediate vicinity of the nematic transition.

Suitably scaled for length and solvent viscosity η_0, the mutual friction is remarkably similar under various conditions. The initial increase in f_m with concentration was considered by Goinga and Pecora[93] and Itou et al.,[94] based on the approximate theory of Peterson.[95] It is easy to convert eqs 5 and 11 of ref 93 to our reduced number

density concentration scale. If $f_m = f_m^\circ(1 + k^*_{f_m}(\nu/\nu^*) + ...)$, then $k^*_{f_m} = (64/3)^{1/3}k_BT/(\pi\eta_0 D^\circ L^{2/3}d^{1/3})$. It will suffice to use the simple Kirkwood–Riseman expression (ref 96 or 57) for D°, leading to

$$k^*_{f_m} = \frac{(576L/d)^{1/3}}{\ln(L/d)} \approx \frac{8.32(L/d)^{1/3}}{\ln(L/d)} \qquad (25)$$

The denominator and numerator both depend weakly on L/D. For the polymers studied here, $k^*_{f_m}$ varies only from 6.3 to 8.3 (a hydrodynamic diameter of 2 nm[19] was used, but this choice is noncritical). Allowing for the normalization of data in Figure 9 to $\eta_0 L$ rather than to f_m°, the initial slopes in Figure 9 should be $(3\pi/\ln(L/d))k^*_{f_m}$, or 17–19 except for PBLG-60 000 (slope ≈ 24). It is almost surprising, given the approximate nature of the Peterson theory,[95] that the initial slopes of Figure 9 are in such good agreement with these expectations, as can be seen by simple inspection. Above $\nu/\nu^* \approx 1/8$, f_m increases more slowly with concentration. The rapid initial rise of f_m below this point may correspond to the loss of perpendicular motions. A general theory of $D_\perp$ has appeared,[97] but Brownian dynamics simulations[98] are perhaps more illuminating. For $x = 50$, they show that 75% of the lateral motions are quenched at $\nu/\nu^* \approx 1/8$.

There is one apparent inconsistency in the above analysis: D_m in Figure 8d does not decrease at $T = 75$ °C, as expected from the osmotic modulus downturn in Figure 1. This is unlike the behavior at $T = 30$ °C. Throughout this discussion, we have been subject to the simplest possible interpretation via eqs 12 and 13. The larger error bars in Figure 8 for the highest concentrations shown at each temperature reflect precision problems related to increasing nonexponential character as concentration is raised. Points at still higher concentrations are not shown at all because of severe nonexponentiality. Thus, although the foregoing analysis is substantially correct, perhaps a more detailed picture will emerge upon consideration of the true character of the correlation functions.

(b) Nonexponential Character of Correlation Functions. Dilute Solutions: Low qL. The correlation functions were nearly single exponential below $\nu/\nu^* \approx 0.2$. Figure 10 shows a correlation function of just-moderate quality for a sample at low concentration ($\nu/\nu^* \approx 0.016$) and low scattering vector ($qL \approx 1.4$). Small, but significant, curvature is evident in the semilogarithmic representation (Figure 10C). The upper of the two curves in Figure 10B represents $g^{(1)}(\tau)$, which can be expressed as a weighted infinite sum of exponential decays:

$$g^{(1)}(\tau) = \int_0^\infty A(\Gamma)e^{-\Gamma\tau}\,d\Gamma \qquad (26)$$

Algorithms developed to perform the difficult[99] task of inverting eq 26 to obtain the amplitude function $A(\Gamma)$ usually return amplitudes at a discrete set of frequencies $\{\Gamma\}$ spaced evenly on a logarithmic scale. Typically, 30–60 decay functions create the impression of a continuous distribution. We denote by $A\{\Gamma\}$ approximate representations of $A(\Gamma)$ obtained by either the smoothed exponential sampling EXSAMP or CONTIN computer programs.[63,68-70] The interactive EXSAMP is used to suggest appropriate parameters for CONTIN, which automatically chooses from among several solutions that one which supposedly is the least detailed distribution consistent with the data.

Figure 11 shows four different results derived from the data in Figure 10. A unimodal distribution is clearly indicated (the small "sidebands" at high decay rates are probably meaningless in this case). There is good agreement between the simple 3CUMU and 1EXP fits and the more elaborate, and reasonably sharp, Laplace inversion distributions. The polydispersity parameter $\mu_2/\bar{\Gamma}^2$ was typically 0.1–0.2. Others have suggested that the ratio of weight- to number-average molecular weights for rodlike polymers can be approximated as $1 + \mu_2/\bar{\Gamma}^2$,[17] implying $M_w/M_n \approx 1.1$–1.2 for the samples studied here. Given the dependence of D° upon M and the dependence of $A\{\Gamma\}$ on concentration, molecular weight, and size, it is possible to

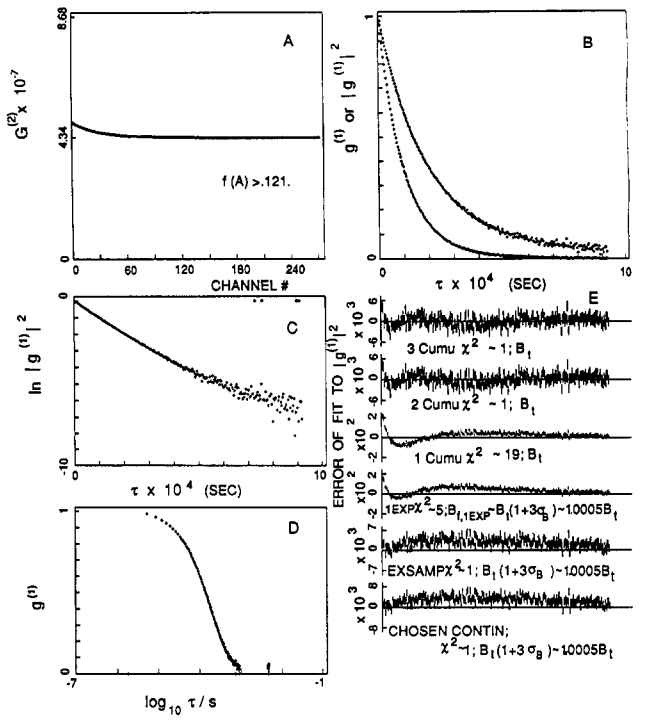

Figure 10. Typical low-c, low-qL correlation function in several representations. PBLG-149 000; $\theta = 45°$; $\lambda_0 = 488$ nm; $T = 40$ °C; $c = 1.603 \times 10^{-3}$ g/mL ($\nu/\nu^* = 0.016$). (A) Raw data, demonstrating just-moderate signal over baseline. (B) Normalized first- and second-order representation after subtraction of B_t. (C) Semilogarithmic representation of second-order normalized correlation function, showing limited and gentle curvature due to polydispersity. (D) $g^{(1)}(\tau)$ as a function of log τ, showing unimodal decay profile. (E) The height of each bar indicates the uncertainty in a given channel. The distance from the center of the bar to the line of zero error represents the difference between actual and fitted values of $|g^{(1)}|^2$, calculated using B_t. The residuals lie systematically above the line of zero error for 1EXP, EXASAMP, and CONTIN, calling attention to the minor baseline adjustments employed in these fits; χ^2 was computed with the adjusted baseline. The abscissa is the same as in panel B.

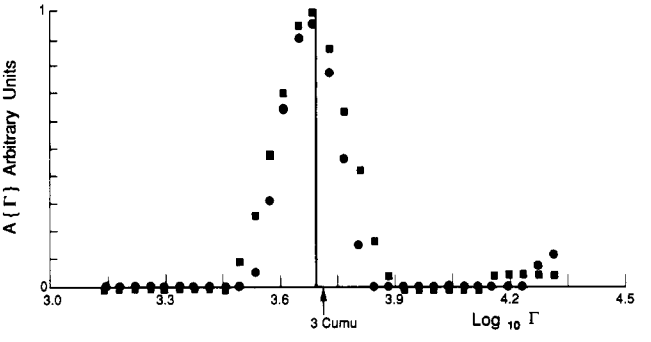

Figure 11. Distribution of scattering amplitude against decay rate, obtained by CONTIN (circles) and EXSAMP (squares) for the same sample as in Figure 10. The error bars for the amplitudes are smaller than the points. The weak, fast peak is probably insignificant. The vertical line shows the decay rates of a single peak from 1EXP, with floated baseline; the arrow locates the 3CUMU value.

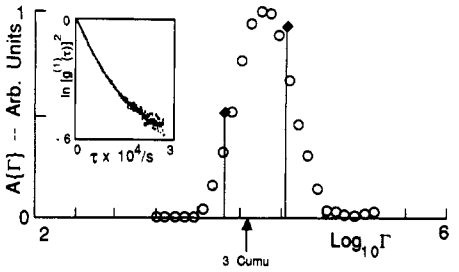

Figure 12. CONTIN distribution for a typical sample at intermediate concentrations. The error bars for the amplitudes are smaller than the points. The vertical lines show the decay rates from 2EXP using baseline B_t; line heights indicate relative mode amplitudes. The arrow locates the 3CUMU decay rate; computed without any baseline adjustment, it tends somewhat toward the slow side of the distribution in this case, but is still within about 20% of the average decay rate.

convert from $A\{\Gamma\}$ to $c\{M\}$. Without going into details,[100] doing this confirms that M_w/M_n of about 1.1–1.2 is reasonable for these samples.

Dilute Solutions: Moderate *qL*. Despite the positive curvatures of Figure 5, actual resolution of the two decay modes was difficult and imprecise. For the largest fraction, the faster rotational–diffusion mode of eq 14 accounted for about 10% of total decay amplitude at $qL \approx 5$, and D_r was found to be 3800 ± 400 Hz. This is at least comparable to the predictions of Kirkwood and Riseman or Broersma[96,101] (see also ref 57), assuming a hydrodynamic rod diameter of 2 nm (3600 and 3100 Hz, respectively). This analysis ignores translational–rotational coupling and flexibility.

Solutions at Intermediate Concentrations. In the concentration regime $0.2 < \nu/\nu^* < 0.7$, there is increasing nonexponentiality, but only scant evidence of the very slow decay mode that occurs at still higher concentrations. Figure 12 shows a typical CONTIN distribution for a sample in this regime. The distribution from EXSAMP, not shown, is just slightly wider. The semilogarithmic plot of the correlation function (inset) shows slightly greater curvature than in dilute solution (compare Figure 10C). The discrete 2EXP fit was essentially as good as the CONTIN or EXSAMP quasicontinuous distributions, the normalized residuals χ^2 in each case being 1–3 with very low channel-to-channel correlation. The small arrow shows the most important feature—that the 3CUMU fit still provides a reasonable representation of the average decay rate. In fact, the 3CUMU fit was as successful as 2EXP, CONTIN, or EXSAMP (not shown) in the particular case of Figure 12, which represents the middle of the intermediate regime.

Concentrated Solutions. When $\nu/\nu^* > \approx 0.7$ a very slow decay mode becomes prominent. It is exceedingly unlikely that this has to do with "dust", for the samples are prepared by concentration of dilute or intermediate specimens that display no strong slow modes. In some cases, the very slow mode is visible as a bright speckle pattern when the laser beam is observed traversing the sample at 100× magnification, using the microscope facilty of the detector. At the highest concentrations, the speckle pattern is virtually stationary. It is evident in samples aged for well over 1 year and is probably not due to incomplete mixing.

(c) A Classification Scheme for Nonexponentiality in the Intermediate and Concentrated Regimes. A letter designation will be used to distinguish experimentally observed modes from theoretically predicted ones, to which we will give numeric identifiers. The very slowly decaying mode just discussed is called mode A, with decay rate Γ_A and amplitude A_A. Additional characteristics of mode A are revealed in Figures 13 and 14. The amplitude A_A increases with concentration, decreases with scattering angle, and can comprise more than 40% of the structure factor. It seems to decrease slightly with temperature, although this effect is not pronounced (and not shown). With our present correlator, it would be difficult to measure Γ_A at any scattering angle, let alone its angular dependence.

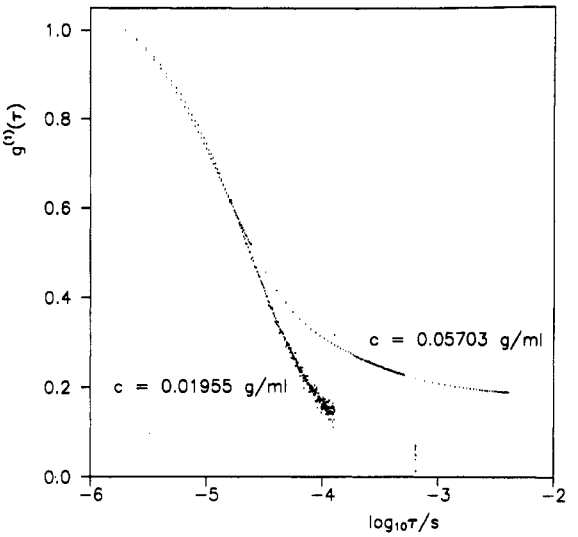

Figure 13. First-order correlation functions for PBLG-277 000 at T a= 75 °C, $\theta = 120°$, and $\lambda_0 = 488$ nm at two concentrations, indicated. Mode A (see text) is evident at the higher concentration, necessitating the use of the multi-τ feature of the correlator, while at the lower concentration, there is a smooth decay into noise and linear operation is adequate.

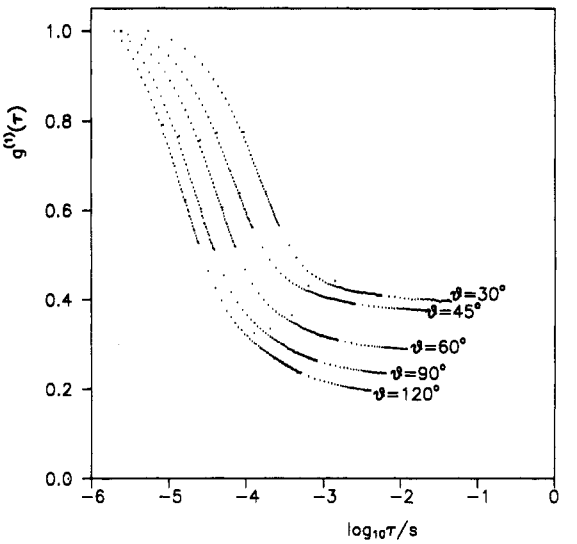

Figure 14. First-order correlation functions for PBLG-277 000 at c = 0.0570 g/mL at various angles, indicated. Mode A (see text) is more pronounced at low angles.

We may classify the other observed modes alphabetically in order of ascending decay rate with the help of Figure 15, which shows CONTIN distributions at various concentrations. A scattering angle of 120° was chosen to reduce the contribution of mode A. In each case, the theoretical baseline B_t was used. The chosen CONTIN distribution is shown except at the lowest concentration, where the eighth sequential distribution, equally successful at fitting the data, provides more detail (at the penalty of substantial amplitude uncertainties).

Mode B is much faster than mode A, and mode C is considerably faster and somewhat stronger yet. The weak

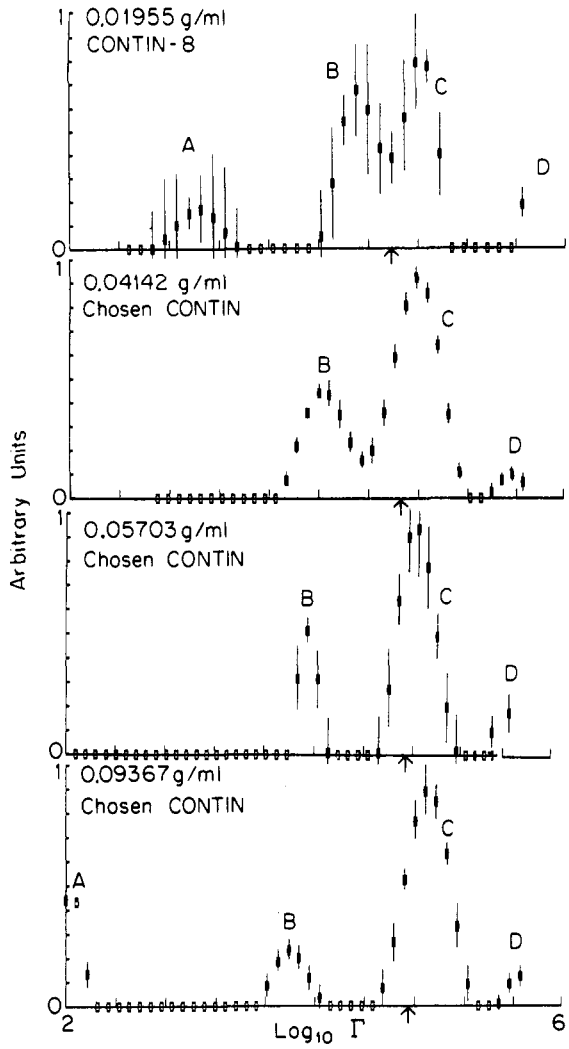

Figure 15. CONTIN distributions for four concentrations at 75 °C and $\theta = 120°$. Decay modes are shown by capital letters; see text. In order not to crowd modes B and C, mode A does not appear in its entirety, except at the lowest concentration.

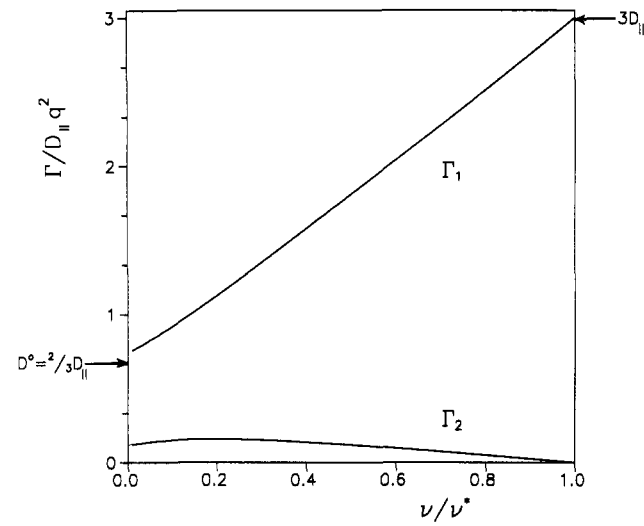

Figure 16. Decay rates predicted by the DSO model; scaled by q^2 and $D_\parallel$ (see text). Dilute solution and Doi–Edwards expectation values of D_m at $\nu = \nu^*$ are shown. Note that Γ_2 tends to zero at $\nu = \nu^*$.

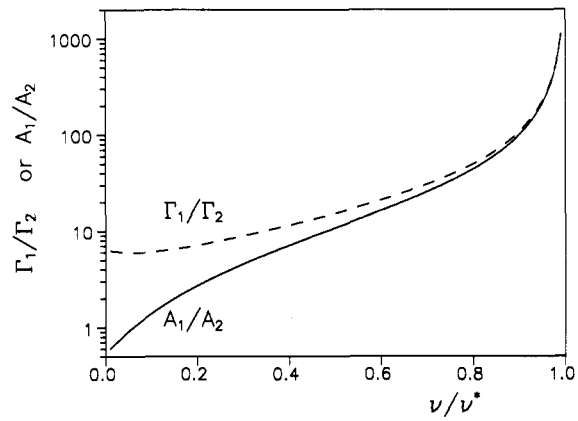

Figure 17. Ratios of decay rates and mode amplitudes from the DSO model. Amplitude values below $\nu/\nu^* \approx 0.3$ are probably not meaningful (see text).

and even faster mode D is present only when mode A is, but is curiously absent from EXSAMP fits. Mode D is very sensitive to selection of baseline and other parameters of the Laplace inversion algorithm, such as the range in Γ space over which solutions are sought, the number of grid points, etc. It will not be discussed further.

(d) Interpretation of Nonexponentiality. To determine which (if any) of the four modes agree with the bimodal DSO prediction, eq 4.12 (subject to eq 4.8) of ref 15 are plotted in Figure 16, where the decay rates are scaled by $D_\parallel q^2$ ($=D_\parallel^\circ q^2$ in the model). On this scale, the expectations for mutual diffusion at $\nu/\nu^* = 0$ and 1 are, respectively, $^2/_3$ and 3, as already discussed in section Va. It is clear that the correlation function must be dominated by mode 1 at both low and high concentrations in order for these expectations to be met. Shown in Figure 17 are the calculated amplitude and decay rate ratios. The amplitudes appear to be inaccurate at low concentration, with A_2 exceeding A_1. DSO drew a decay time curve, their Figure 3, with a dashed line below $\nu/\nu^* \approx 0.3$, perhaps indicating some unspecified uncertainty about the validity of the theory in this regime. According to the foregoing, the assumption $D_\perp = 0$ is suspect below $\nu/\nu^* \approx 0.3$. Anyway, the behavior at $\nu/\nu^* > 0.3$ seems reasonable. Ultimately, mode 2 becomes much weaker and slower than mode 1, but at intermediate concentrations, mode 1 is about 5–20 times faster than mode 2 and its amplitude is about 4–10 times larger. The mode amplitudes are independent of scattering angle in the DSO model.

Experimental mode A becomes very slow with increasing concentration, as predicted for theoretical mode 2. However, we do not feel that mode A corresponds to mode 2, because its amplitude increases with concentration and depends on scattering angle. We tentatively group mode A with the increased correlation length and turnaround of osmotic modulus—two other observations not predicted by DSO theory. If the increased correlation length and turnaround of osmotic modulus represent the limitations of a mean field approach, then perhaps mode A signals the dynamic limitations.

From the CONTIN representation in Figure 15, it seems that modes B and C behave respectively like modes 2 and 1. Mode B shifts toward lower decay rates with concentration, becoming relatively weaker in the process, while mode C does the opposite. To examine this in greater detail, mode A was effectively "subtracted out" from the correlation functions. This was accomplished by computing $g^{(1)}(\tau)$ using a baseline obtained from a fit to $G^{(2)}(\tau)$ with two or three exponentials (note: as it contains the square of $g^{(1)}(\tau)$, $G^{(2)}(\tau)$ cannot actually have just two exponentials; this practice is just a means of estimating a baseline). In the terminology established earlier, a 2EXP fit was made to $g^{(1)}(\tau)$ computed using the baseline $B_{f,2EXP}$ or $B_{f,3EXP}$. The baselines so obtained corresponded closely

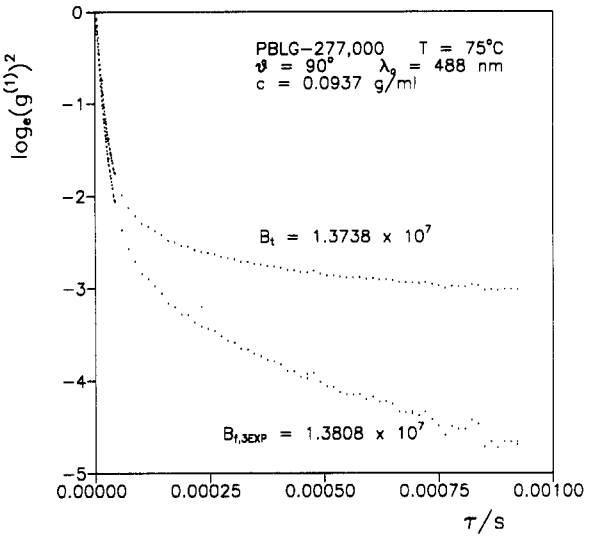

Figure 18. First-order correlation functions for PBLG-277 000 at T = 75 °C, θ = 90°, and λ_0 = 488 nm. Only the first two functions obtained during multi-τ operation of the correlator are shown. When the correlation function is computed with B_t, the "leveling" effect due to very slow mode A is evident. When a fitted baseline, $B_{f,3EXP}$, is employed, two distinct regimes are clearly evident indicating a strong, fast mode (mode C) and a weaker and slower mode (mode B).

to the plateau values prior to the A-mode relaxation (see Figures 13 and 14). Figure 18 displays the recomputation of $g^{(1)}(\tau)$ and demonstrates that with mode A subtracted, the remaining correlation function is approximately biexponential. The primary limitation to the reliability of the 2EXP fits under these unusual circumstances was baseline uncertainty. Recomputation with several baselines slightly different from $B_{f,3EXP}$ showed that the slower and weaker mode B was affected more than mode C. Amplitudes varied with reasonable baseline changes by about ±20% and ±7% for modes B and C, respectively. Decay rates varied by about ±30% and ±5%. Figure 19 shows the q dependence of modes B and C determined in this way at various concentrations. As predicted,[15] both modes are diffusive, scaling linearly with q^2. Overall, the slopes of the mode C plots appear to increase with concentration, but somewhat erratically and hardly as much as expected from Figure 16. This behavior is similar to the mild increases in the average decay rate (Figure 8) and reaffirms our suspicions about the constancy of $D_\parallel$. In contrast, mode B slopes decrease strongly with concentration and are some 7–30 times slower than mode C. This factor is comparable to the expectations of Figure 16; however, given the too-slow increase of mode C, it is hard to claim agreement. The amplitude ratio at the lowest angle appears higher than at others (Figure 20). However, within the considerable uncertainties, there is no significant change with angle or concentration, unlike mode A, but in agreement the DSO theory. The ratio hovers near 2–3, a little lower than predicted.

The limitations of the 2EXP, multiangle analysis (and, ultimately, the need to resolve mode A fully) are evident upon comparing Figures 15 and 19b. Although CONTIN reported a small difference in mode B between the two highest concentrations, the 2EXP analysis after substantial baseline adjustment does not. Nonetheless, it is certain that mode B slows dramatically with concentration. Similarly, the mode C slopes of Figure 19a increase with concentration, but not monotonically as in Figure 15. Nevertheless, the diffusive nature and overall concentration dependence of decay rates and amplitudes of modes B and C do resemble DSO modes 2 and 1, respectively.

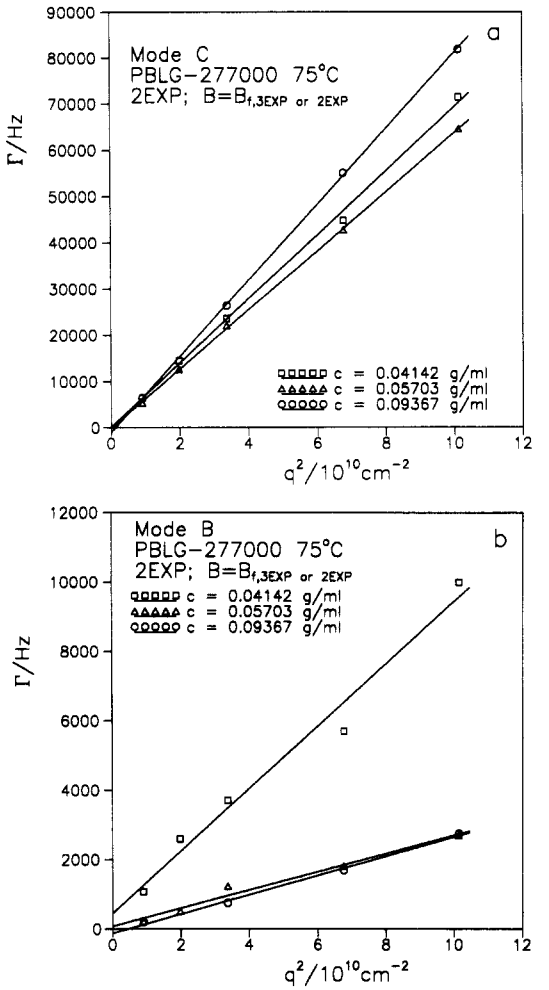

Figure 19. (a) Γ_C scales linearly with q^2, and the intercept is zero, within error. The overall trend is toward increasing Γ with increasing concentration. (b) Γ_B also scales linearly with q^2; given the uncertainties associated with this mode (see text), the intercepts are probably zero, within error. The trend is definitely toward decreasing Γ_C with increasing concentration.

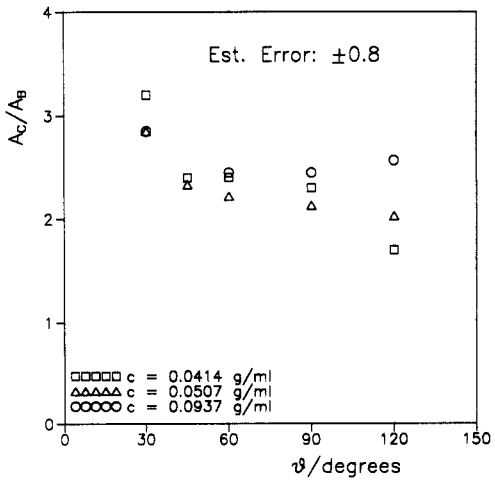

Figure 20. Ratio of A_C/A_B against scattering angle; same samples as in Figure 19. Estimated uncertainty is ±0.8.

The principal failings of the DSO model are its inability to predict mode A and the assumption that $D_\parallel$ is constant. Otherwise, the qualitative agreement between experimentally observed modes B and C and DSO modes 2 and 1 suggests that the model has some merit. Elsewhere,[57] a heuristic physical picture of the dynamic scattering model is provided. Briefly, the two modes—one becoming slower

and weaker with concentration—are related to the coupling of orientation and concentration fluctuations. Note that this is not the same molecular rotational–translational coupling that occurs in dilute solution.[54-58] Though consistent with dilute solution theories at the first-cumulant level (see eqs 16–21), the DSO formalism generalizes to high concentrations. The two modes reflect that the concentration fluctuations observed by polarized light scattering can arise and decay with or without changes in intermolecular orientation. The rates of these two processes depend on anisotropic molecular mobilities (as in the original Doi–Edwards model[59,60]) but also upon thermodynamic factors. In particular, relaxations away from an aligned state become critically slowed near the nematic, and so concentration changes coupled to disalignments are no longer "competitive" compared to relaxation processes that leave alignment unchanged. These latter processes, which at the molecular level rely upon on a (relatively) unhindered $D_{\parallel}$ and are actually hastened by excluded volume interactions, thus account for an increasing portion of the relaxation of the correlation function.

(e) Depolarized Dynamic Light Scattering. At intermediate concentrations, the depolarized signal level was sufficient that a relatively noise-free correlation function at a given angle could be measured within a 24-h period. Within a week, the angular dependence of $\bar{\Gamma}$ could be obtained. Extremely unusual behavior was repeatedly observed under many conditions, but only at high concentrations.[87] Although there are some depolarized measurements at $\theta = 90°$,[16,17] there appears to be only one other angle-dependent depolarized light scattering study of semidilute rods,[102] with somewhat less unusual but still confounding results that may stem from molecular asymmetry.

VI. Concluding Remarks

In this paper, many features of the classical Onsager and random phase theories for rods in solution have been verified. An important attribute of the random phase theory is its ability to handle dynamic processes, including the first rational model for (athermal) spinodal decomposition in rod-bearing systems.[15] For various reasons,[83] true spinodal decomposition may be difficult to observe. Nevertheless, the present results lend enough support to the underlying model to suggest that it is conceptually valid at least as an initial mechanism of phase separation of rod-bearing solutions.

The concern sometimes expressed[7] about the effects of finite solvent size seem not to materialize in PBLG/DMF, as the measured virial coefficients imply a diameter quite close to any reasonable expectation and to independent measurement.[77]

There is still room for improvement in the theory of both static and dynamic properties. The rather low rate of decrease in static correlation length with concentration, as well as the sudden increase as the nematic is approached, the existence of the very slow mode A, and the exact behavior of the osmotic modulus at high concentrations certainly deserve further theoretical attention. The same is true of flexibility, the effects of which are more evident at high concentrations than low. The ability to exploit this for the determination of persistence lengths in the fairly stiff limit lacks only an appropriate theory of the first cumulant.

On the experimental side, additional angle-dependent depolarized data would be desirable. Orientational structuring may be evident at very low scattering angles, as in another rod-bearing suspension.[102] Maeda's extension of the DSO theory[62] suggests that excluded volume effects may be weaker in depolarized dynamic light scattering than in polarized, so details associated with molecular architecture can be explored more directly. As for the polarized scattering, the main requirement is better resolution of the slow decay modes and their comparison with the viscoelastic spectrum, which has proven illuminating in random coil systems.[103] Although ξ was in close agreement with expectations up to $\nu/\nu^* \approx {}^7/_{27}$, where the sign of the term describing the q^4 dependence of $g(q)$ changes, further detail can probably be accomplished with small-angle X-ray scattering experiments, already underway.

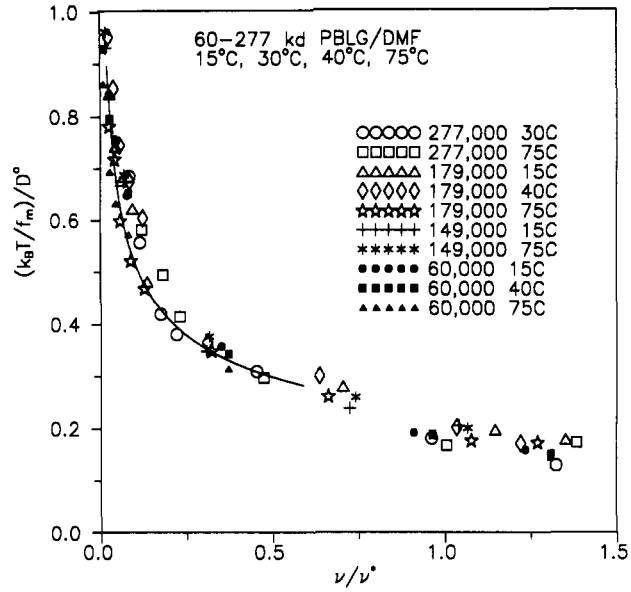

Figure 21. Ratio of thermal energy to mutual friction coefficient, divided by diffusion coefficient in the dilute limit, can be scaled by ν^*. Brownian dynamics simulations of Bitsanis et al.[98] for $x = 50$ are also shown as a smooth line.

We conclude with an intriguing observation. The data in Figure 9 can be replotted as k_BT/f_m vs ν/ν^*. If $f_m \approx f_s$, this would resemble the concentration dependence of D_s. As shown in Figure 21, all the data fall on the same curve with no adjustable parameters. The plot agrees perfectly with Brownian dynamics simulations[98] for $x = 50$. However, only a few true measurements of D_s for rods are known[104-106] and none in the same range of x and L/a. Preliminary fluorescence photobleaching recovery[107] measurements in this laboratory of an end-labeled PBLG with axial ratio ≈6 dispersed in pyridine show a steeper decline of D_s with concentration than Figure 21; D_s ultimately reaches about $D^\circ/10$ at 40 wt %. The low axial ratio of this sample may exacerbate finite thickness effects or interfere with the shielding of hydrodynamic interactions, causing the rapid decline of D_s with c. It will not be possible to judge the utility of Figure 21 until the completion of similar but more difficult experiments on longer PBLG's and expensive Brownian dynamics simulations at higher axial ratio.

Acknowledgment. This work was supported by grants from the Polymers Program, Division of Materials Research, National Science Foundation (Grants DMR-8520027 and DMR-89-14604). We are also indebted to Professors Randall Hall and Dewey Carpenter of this department and Dr. Tadakazu Maeda of the Mitsubishi Kasei Institute of Life Sciences for many valuable insights. We are grateful to the reviewers who toiled with an even longer version of this paper.

Supplementary Material Available: Detailed preparative and measurement methods for the PBLG samples used in this study (7 pages). Ordering information is given on any current masthead page.

Appendix

Equation 10 can be derived without resort to the random phase formalism. Equation 1 is easily rewritten as

$$Kc/\mathcal{R} = M^{-1}(1 + 2\nu A_{2,\nu} + ...)(1 + \xi^2 q^2 + ...) \quad (A1)$$

Setting this equal to the classical Zimm expression, eq 2, and comparing coefficients of q^2 yield

$$\xi^2 = (R_g{}^2/3)/(1 + 2\nu A_{2,\nu} + ...) \quad (A2)$$

Remembering that $R_g{}^2 = L^2/12$ for rods and also the Onsager/Zimm/Schulz prediction that $A_{2,\nu} = 4/\nu^*$ (with $A_{3,\nu}$ and higher order terms being 0), we obtain eq 10. This exercise demonstrates the equivalence of the DSO random phase formalism to earlier treatments of the excluded volume problem in rods and to the classical theory of light scattering of finite concentrations.

References and Notes

(1) Bawden, F. C.; Pirie, N. W.; Bernal, J. D.; Fankuchen, I. *Nature* **1936**, *138*(2), 1051.
(2) Robinson, C. *Trans. Faraday Soc.* **1956**, *52*, 571.
(3) Robinson, C.; Ward, J. C.; Beevers, R. B. *Discuss. Faraday Soc.* **1958**, *25*, 29.
(4) Robinson, C. *Mol. Cryst.* **1966**, *1*, 467.
(5) Onsager, L. *Ann. N.Y. Acad. Sci.* **1949**, *51*, 627.
(6) Flory, P. J. *Proc. R. Soc. London, Ser. A* **1956**, *234*, 73.
(7) Flory, P. J.; Ronca, G. *Mol. Cryst. Liq. Cryst.* **1979**, *54*, 289.
(8) Flory, P. J. In *Polymer Liquid Crystals*; Ciferri, A., Krigbaum, W. R., Meyer, R. B., Eds.; Academic Press: New York, 1982; Chapter 4.
(9) Miller, W. G. *Annu. Rev. Phys. Chem.* **1978**, *29*, 519.
(10) *The Materials Science and Engineering of Rigid Rod Polymers*; Adams, W. W., Eby, R. K., McLemore, D. E., Eds.; Materials Research Society: Pittsburgh, 1989.
(11) Odijk, T. *Macromolecules* **1986**, *19*, 2313.
(12) Hentschke, R. *Macromolecules* **1990**, *23*, 1192.
(13) Shimada, T.; Doi, M.; Okano, K. *J. Chem. Phys.* **1988**, *88*, 2815.
(14) Doi, M.; Shimada, T.; Okano, K. *J. Chem. Phys.* **1988**, *88*, 4070.
(15) Shimada, T.; Doi, M.; Okano, K. *J. Chem. Phys.* **1988**, *88*, 7181.
(16) Zero, K.; Pecora, R. *Macromolecules* **1982**, *15*, 87.
(17) Kubota, K.; Chu, B. *Biopolymers* **1983**, *22*, 1461.
(18) Schmidt, M. *Macromolecules* **1984**, *17*, 553.
(19) Russo, P. S.; Karasz, F. E.; Langley, K. H. *J. Chem. Phys.* **1984**, *80*, 5312.
(20) Kubota, K.; Tominaga, Y.; Fujime, S. *Macromolecules* **1986**, *19*, 1604.
(21) Block, H. *Poly(γ-benzyl L-glutamate) and Other Glutamic Acid Containing Polymers*; Gordon and Breach: New York, 1983.
(22) See, for example: Yamakawa, H. *Modern Theory of Polymer Solutions*; Harper and Row: New York, 1971; Section 9c.
(23) Saba, R. G.; Sauer, J. A.; Woodward, A. E. *J. Polym. Sci.* **1963**, *A1*, 1483.
(24) Koleske, J. V.; Lundberg, R. S. *Macromolecules* **1969**, *2*, 438.
(25) Hiltner, A.; Anderson, J. M.; Borkowski, E. *Macromolecules* **1972**, *5*, 446.
(26) Tschoegl, N. W.; Ferry, J. *J. Am. Chem. Soc.* **1964**, *86*, 1474.
(27) Iwata, K. *Biopolymers* **1980**, *19*, 125.
(28) Aharoni, S. M. *Macromolecules* **1983**, *16*, 1722.
(29) Yamakawa, H. *Annu. Rev. Phys. Chem.* **1984**, *35*, 23.
(30) Crosby, C. R., III; Ford, N. C.; Karasz, F. E.; Langley, K. H. *J. Chem. Phys.* **1981**, *75*, 4298.
(31) Farmer, B.; Adams, W. W. *Bull. Am. Phys. Soc.* **1990**, *35* (3), 508.
(32) This term is used by at least one active group to distinguish linear extended backbone rods from helical polymers such as PBLG or aramid type backbone polymers.
(33) Einstein, A. *Ann. Phys.* **1910**, *33*, 1275.
(34) Debye, P. *J. Phys. Colloid Chem.* **1947**, *51*, 18.
(35) Zimm, B. H. *J. Chem. Phys.* **1948**, *16*, 1093.
(36) Our preference for "osmotically stiff" over "high modulus" was not shared by the referees. However, it may be helpful to think of solutions in good solvents far from phase separation as "stiff" and solutions nearer to phase boundaries as "soft" with regard to concentration fluctuations.
(37) Zimm, B. *J. Chem. Phys.* **1946**, *14*, 164.
(38) Schulz, G. V. *Z. Naturforsch.* **1947**, *2a*, 348.
(39) Edwards, S. F. *Proc. R. Soc. London* **1966**, *88*, 256.
(40) de Gennes, P.-G. *J. Phys. (Paris)* **1970**, *31*, 235.
(41) Ten Bosch, A.; Sixou, P. *J. Chem. Phys.* **1985**, *83*, 899.
(42) de Gennes, P.-G. *Scaling Concepts in Polymer Physics*; Cornell University Press: Ithaca, NY, 1979; Chapter 3.
(43) Daoud, M.; Cotton, J. P.; Farnoux, B.; Jannink, G.; Sarma, G.; Benoit, H.; Duplessix, R.; Picot, C.; de Gennes, P.-G. *Macromolecules* **1975**, *8*, 804.
(44) Doi, M.; Edwards, S. F. *The Theory of Polymer Dynamics*; Clarendon Press: Oxford 1986; Chapters 8–10.
(45) de Gennes, P.-G.; Pincus, P.; Velasco, R. M.; Brochard, F. *J. Phys. (Paris)* **1976**, *37*, 1461.
(46) Muthukumar, M.; Edwards, S. F. *Macromolecules* **1983**, *16*, 1475.
(47) Odijk, T. *Macromolecules* **1986**, *19*, 2073.
(48) Berne, B.; Pecora, R. *Dynamic Light Scattering*; Wiley: New York, 1976.
(49) Schmitz, K. S. *An Introduction to Dynamic Light Scattering by Macromolecules*; Academic Press: San Diego, 1990; Chapter 3.
(50) See, for example: Yamakawa, H. *Modern Theory of Polymer Solutions*; Harper and Row: New York, 1971; Section 30b.
(51) Schurr, J. M. *Chem. Phys.* **1987**, *111*, 55.
(52) See, for example: Callaghan, P. T.; Pinder, D. N. *Polym. Bull. (Berlin)* **1981**, *5*, 305.
(53) Koppel, D. E. *J. Chem. Phys.* **1972**, *57*, 4814.
(54) Schmidt, M.; Stockmayer, W. H. *Macromolecules* **1984**, *17*, 509.
(55) Wilcoxon, J. P.; Schurr, J. M. *Biopolymers* **1983**, *22*, 849.
(56) Maeda, T.; Fujime, S. *Macromolecules* **1984**, *17*, 1157.
(57) Russo, P. S. In *Dynamic Light Scattering, the Method and Some Applications*; Brown, W., Ed.; Oxford: New York, in press.
(58) Schurr, J. M.; Schmitz, K. S. *Annu. Rev. Phys. Chem.* **1986**, *37*, 271.
(59) Doi, M.; Edwards, S. F. *J. Chem. Soc., Faraday Trans. 2* **1978**, *74*, 560.
(60) Doi, M.; Edwards, S. F. *J. Chem. Soc., Faraday Trans. 2* **1978**, *74*, 918.
(61) Maeda, T. *Macromolecules* **1989**, *22*, 1881.
(62) Maeda, T. *Macromolecules* **1990**, *23*, 1464.
(63) Russo, P. S.; Saunders, M. J.; DeLong, L. M.; Langley, K. H.; Detenbeck, R. W.; Kuehl, S. *Anal. Chim. Acta* **1986**, *189*, 69.
(64) Russo, P. S.; Stephens, L. K.; Cao, T.; Mustafa, M. *J. Colloid Interface Sci.* **1988**, *122*, 120.
(65) Kaye, W.; McDaniel, J. B. *Appl. Opt.* **1974**, *13*, 1934.
(66) Leite, R. C. C.; Moore, R. S.; Porto, S. P. S.; Ripper, J. E. *Phys. Rev. Lett.* **1965**, *14*, 7.
(67) Bevington, P. R. *Data Reduction and Error Analysis for the Physical Sciences*; McGraw-Hill: New York, 1969.
(68) Ostrowski, N.; Sornette, D.; Parker, P.; Pike, E. R. *Opt. Acta* **1981**, *28*, 1059.
(69) Russo, P.; Guo, K.; DeLong, L. M. *Proceedings of the 46th Annual Technical Conference of the Society of Plastics Engineers*, **1988**, p 983. Supplemental information is available from the authors.
(70) Provencher, S. W. *Comput. Phys.* **1982**, *27*, 213, 229.
(71) See, for example: Kratochvil, P. In *Light Scattering from Polymer Solutions*; Huglin, M. B., Ed.; Academic Press: New York, 1972; Chapter 7.
(72) Goebel, K. D.; Miller, W. G. *Macromolecules* **1970**, *3*, 64.
(73) Kubo, K.; Ogino, K. *Mol. Cryst. Liq. Cryst.* **1979**, *53*, 207.
(74) Russo, P. S.; Miller, W. G. *Macromolecules* **1984**, *17*, 1324.
(75) Watanabe, J.; Imai, K.; Uematsu, I. *Polym. Bull. (Berlin)* **1978**, *1*, 67.
(76) Mitchel, J. C.; Woodward, A. E.; Doty, P. *J. Am. Chem. Soc.* **1957**, *79*, 3955.
(77) Abe, A.; Yamazaki, T. *Macromolecules* **1989**, *22*, 2138.
(78) Khoklov, A. R.; Semenov, A. N. *Physica* **1982**, *112A*, 605.
(79) Tipton, D. L.; Russo, P. S., work in progress.
(80) Miller, W. G.; Wu, C. C.; Wee, E. L.; Santee, G. L.; Rai, J. H.; Goebel, K. G. *Pure Appl. Chem.* **1974**, *38*, 37.
(81) Russo, P. S.; Miller, W. G. *Macromolecules* **1983**, *16*, 1690.
(82) Teramoto, A.; Sato, T. *Polym. Prepr. (Am. Chem. Soc., Div. Polym. Chem.)* **1990**, *32*(1), 507.
(83) Binder, K. *Colloid Polym. Sci.* **1987**, *265*, 273.
(84) Lee, C. C.; Chu, S.-G.; Berry, G. C. *J. Polym. Sci., Polym. Phys. Ed.* **1983**, *21*, 1573.
(85) Benoit, H.; Stockmayer, W. *J. Phys. Radium* **1956**, *17*, 21. A translation appears in: *Light Scattering from Dilute Polymer Solutions*; McIntyre, D., Gornick, F., Eds.; Gordon and Breach: New York, 1964; Chapter 9.

(86) Du Pre, D. B. In *Polymer Liquid Crystals*; Ciferri, A., Krigbaum, W. R., Meyer, R. B., Eds.; Academic Press: New York, 1982; Chapter 4.
(87) DeLong, L. M. Ph.D. Thesis, Lousiana State University, 1990.
(88) Maeda, T.; Fujime, S. *Macromolecules* **1985**, *18*, 191, 2430.
(89) Song, L.; Kim, U.-G.; Wilcoxon, J.; Schurr, J. M. *Biopolymers*, to appear.
(90) Jamieson, A.; Southwick, J.; Blackwell, J. *J. Polym. Sci., Polym. Phys. Ed.* **1982**, *20*, 1513.
(91) Keep, G. T.; Pecora, R. *Macromolecules* **1988**, *21*, 817.
(92) Pecora, R.; Tracy, M., results presented at the Atlanta, GA, ACS meeting, April 1990.
(93) Goinga, H. T.; Pecora, R. *Macromolecules*, in press.
(94) Itou, S.; Nishioka, N.; Norisuye, T.; Teramoto, A. *Macromolecules* **1981**, *14*, 904.
(95) Peterson, J. M. *J. Chem. Phys.* **1964**, *40*, 2680.
(96) Riseman, J.; Kirkwood, J. G. *J. Chem. Phys.* **1950**, *18*, 512.
(97) Teraoka, I.; Hayakawa, R. J. *J. Chem. Phys.* **1988**, *89*, 6989.
(98) Bitsanis, I.; Davis, H. T.; Tirrell, M. *Macromolecules* **1990**, *23*, 1157.
(99) Bott, S. In *Measurement of Suspended Particles by Quasielastic Light Scattering*; Dahneke, B. E., Ed.; Wiley: New York, 1983.
(100) See, for example: Pope, J. W.; Chu, B. *Macromolecules* **1984**, *17*, 2633.
(101) Broersma, S. *J. Chem. Phys.* **1960**, *32*, 1626, 1632.
(102) Donkai, N.; Schmidt, M.; Kajiwara, K.; Urakawa, H.; Inagaki, H. In *Ordering and Organizing in Ionic Solutions*; World Scientific Publishing Co.: Singapore, and Yamada Science Foundation: Osaka, 1988; p 82.
(103) Nicolai, T.; Brown, W.; Johnsen, R. M.; Stepanek, P. *Macromolecules* **1990**, *23*, 1165.
(104) Tinland, B.; Maret, G.; Rinaudo, M. *Macromolecules* **1990**, *23*, 596.
(105) Scalettar, B. A.; Hearst, J. E.; Klein, M. P. *Macromolecules* **1989**, *22*, 4550.
(106) Miller, W. G., personal communication.
(107) Russo, P. S.; Mustafa, M. B.; Cao, T., work in progress.

Registry No. PBLG (homopolymer), 25014-27-1; PBLG (SRU), 25038-53-3.